

## THE NEAR-EARTH ASTEROID TRACKING (NEAT) PROGRAM: AN AUTOMATED SYSTEM FOR TELESCOPE CONTROL, WIDE-FIELD IMAGING, AND OBJECT DETECTION

STEVEN H. PRAVDO,<sup>1,2</sup> DAVID L. RABINOWITZ,<sup>1</sup> ELEANOR F. HELIN,<sup>1</sup> KENNETH J. LAWRENCE,<sup>1</sup> RAYMOND J. BAMBERY,<sup>1</sup>  
CHRISTOPHER C. CLARK,<sup>1</sup> STEVEN L. GROOM,<sup>1</sup> STEVEN LEVIN,<sup>1</sup> JEAN LORRE,<sup>1</sup> STUART B. SHAKLAN,<sup>1</sup> PAUL KERVIN,<sup>3</sup>  
JOHN A. AFRICANO,<sup>3</sup> PAUL SYDNEY,<sup>3</sup> AND VICKI SOOHOO<sup>3</sup>

Received 1998 September 2; accepted 1998 November 20

### ABSTRACT

The Near-Earth Asteroid Tracking (NEAT) system operates autonomously at the Maui Space Surveillance Site on the summit of the extinct Haleakala Volcano Crater, Hawaii. The program began in 1995 December and continues with an observing run every month. Its astrometric observations result in discoveries of near-Earth objects (NEOs), both asteroids (NEAs) and comets, and other unusual minor planets. Each six-night run NEAT covers about 10% of the accessible sky, detects thousands of asteroids, and detects two to five NEAs. NEAT has also contributed more than 1500 preliminary designations of minor planets and 26,000 detections of main-belt asteroids. This paper presents a description of the NEAT system and discusses its capabilities, including sky coverage, limiting magnitude, and detection efficiency. NEAT is an effective discoverer of NEAs larger than 1 km and is a major contributor to NASA's goal of identifying all NEAs of this size. An expansion of NEAT into a network of three similar systems would be capable of discovering 90% of the 1 km and larger NEAs within the next 10–40 yr, while serving the additional role of satellite detection and tracking for the US Air Force. Daily updates of NEAT results during operational periods can be found at JPL's Web site (<http://huey.jpl.nasa.gov/~spravdo/neat.html>). The images and information about the detected objects, including times of observation, positions, and magnitudes are made available via NASA's *SkyMorph* program.

**Key words:** instrumentation: detectors — minor planets, asteroids — techniques: image processing

### 1. INTRODUCTION

#### 1.1. Overview

The Near-Earth Asteroid Tracking (NEAT) program (Helin et al. 1997) is the first automated system for remotely controlling a telescope, acquiring wide-field images, and detecting near-Earth objects (NEOs). These objects are a subject of much interest in scientific studies because of their effects when they hit Earth (Gehrels 1994) or other planets, and because they contain primeval material from the formation of the solar system (see, e.g., McFadden, Tholen, & Veeder 1989). Their size distributions and orbits reveal the influences of gravitational perturbations and collisions with each other (Rabinowitz 1997a, 1997b). About 500 of these objects are currently known (Minor Planet Center 1999) but 1000–4000 over 1 km in diameter are thought to exist (Rabinowitz et al. 1994). NEAT results contribute to evaluating the hazard posed by NEOs to Earth and provide targets for physical observations and future space missions.

Under an agreement between the US Air Force (USAF) and NASA's Jet Propulsion Laboratory (JPL), California Institute of Technology, JPL is provided access to a wide-field (f/2.2) Ritchey-Chrétien telescope of 1.0 m aperture located at the 3000 m summit of Haleakala Crater on the island of Maui. This is one of several identical telescopes normally used by the Air Force for ground-based electro-optical deep space surveillance (GEODSS) of artificial satellites. Other GEODSS telescopes are located at Haleakala, in Socorro, New Mexico, and on the island of Diego

Garcia in the Indian Ocean.

Each month, on-site operators at Haleakala (contracted by the Air Force) mount a JPL-owned digital camera on the GEODSS telescope. The operators then switch control of the telescope and camera to an on-site workstation computer owned by JPL. Thereafter, the operators' role is to open and close the telescope dome and to start or stop the control software running on the JPL computer. The role of the remote observing team at JPL is to upload a daily script to the on-site computer, instructing the control program where to point the telescope and take exposures. Each area of sky is imaged three times at 15–30 minute intervals, thus yielding image “triplets.” An additional on-site computer, owned by JPL and connected by a high-speed data link to the main controlling computer, automatically identifies asteroids in each triplet based upon their apparent motion relative to the fixed field stars. For each asteroid, the software measures the apparent magnitude and determines astrometric positions. At the end of the night in Maui (beginning of the workday at JPL in California) the JPL team downloads the resulting asteroid images and positional data for visual verification before reporting the observations to the Minor Planet Center in Cambridge, Massachusetts. Figure 1 shows an overview of the NEAT system.

The NEAT program has thus operated successfully every month since 1995 December. As of 1998 April, NEAT is discovering one to two Earth-approaching asteroids larger than 1 km per monthly six-night run, a rate not exceeded by any other search program. In this paper we describe the elements of the NEAT hardware and software that have advanced the state of the art for asteroid detection. We then review the demonstrated performance of our current system, and compare to contemporaneous systems. Finally, we predict the capabilities of a “NEAT network” consisting

<sup>1</sup> Jet Propulsion Laboratory, California Institute of Technology, 4800 Oak Grove Drive, Pasadena, CA 91109.

<sup>2</sup> The research described in this paper was carried out in part by the Jet Propulsion Laboratory, California Institute of Technology, under contract with the National Aeronautics and Space Administration.

<sup>3</sup> USAF Research Laboratories, 535 Lipoa Parkway, Kihei, HI 96753.

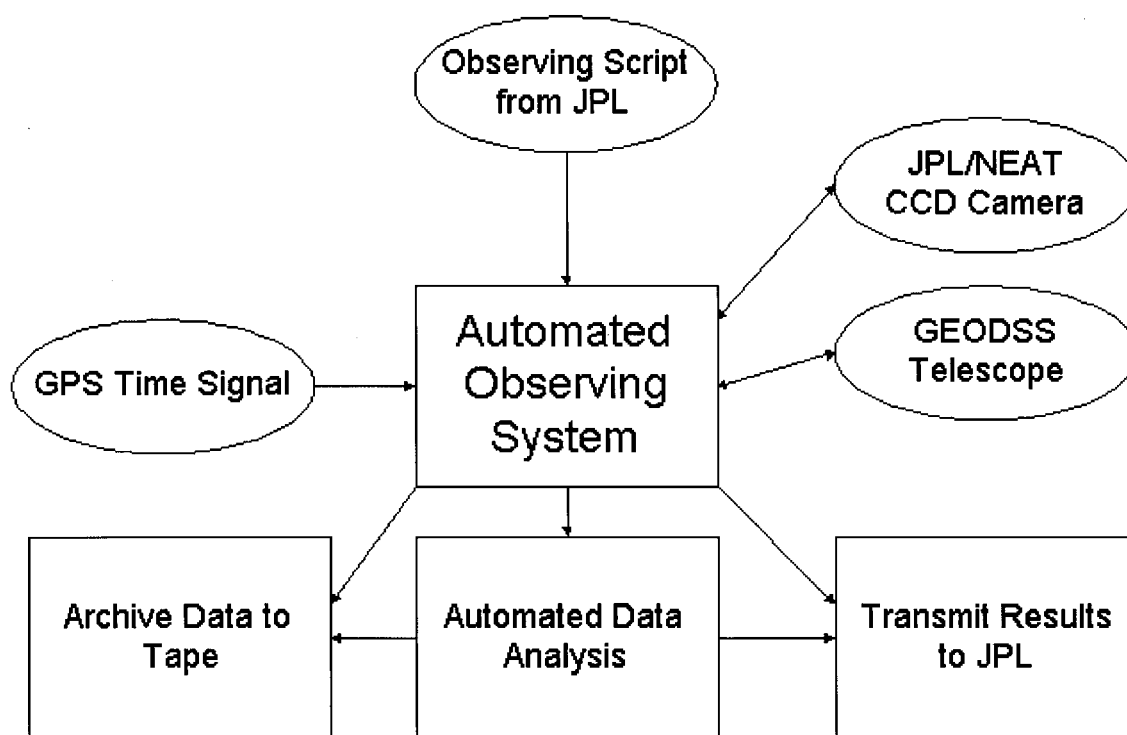


FIG. 1.—NEAT system overview

of the existing system (with improvements) and duplicated on two additional Air Force telescopes. We show that such a system would be capable of detecting 90% of the Earth-approaching asteroids of more than 1 km in 10–40 yr. We also discuss the demonstrated capabilities of the NEAT system for detecting and tracking Earth-orbiting satellites. Such a capability might be required if the NEAT camera were to serve dual use as an asteroid and satellite detector.

### 1.2. *Programmatics and Personnel*

NEAT is a cooperative effort between NASA-JPL and the Air Force Space Command (AFSPC). NASA provides the funds for the JPL-developed camera, computer controller, all the operations and analysis software, and the Science Team. The Science Team at JPL evaluates the data and disseminates the results. Science Team members are Eleanor Helin, Principal Investigator, Steven Pravdo, David Rabinowitz, Co-Investigators, and Kenneth Lawrence. AFSPC provides the site, including the telescope facility and the operations and maintenance personnel. PRC, Inc. has been the contractor performing the operations and maintenance. An AFSPC goal is to evaluate the use of an electronic camera for GEODSS.

The USAF Research Laboratories at Maui (formerly Phillips Laboratory) has participated in the examination of another potential use of NEAT: satellite tracking, the main AFSPC mission for the GEODSS telescopes. NEAT was originally designed to do both asteroid and satellite tracking tasks and is currently being evaluated for the latter (§§ 4.8 and 5.3).

## 2. INSTRUMENTATION

### 2.1. *Camera Hardware*

The NEAT camera was designed and fabricated at JPL in 1995, and its performance has been improved several times

since. It consists of a  $4096 \times 4096$  charge-coupled device (CCD) with  $15 \mu\text{m}$  square pixels, associated control and digitization electronics, a thermoelectric cooler, and a mechanical shutter (see Fig. 2). At the focus of a GEODSS telescope, the pixel scale is  $1''.4$ . In principle, stellar images are undersampled by this pixel size. In practice, the combination of tracking error and seeing (which we have not disentangled) creates images from  $2''.5$  to  $3''$  in diameter, and thus the sampling is adequate. The 4K device covers much of the usable field of view, about  $1''.6$  on a side. As much as  $2^\circ$  could be used, but with further image degradation at the edges.

Digital commands to control the operations of the camera are transmitted via an optical fiber from the on-site workstation computer. A second fiber transmits the returned imaged data to the workstation. An overriding design consideration for the camera was that it fit at the Cassegrain focus, which is a small confined space internal to a GEODSS telescope. This space is usually occupied by an AFSPC video camera, replaced by the JPL camera during NEAT operations.

The NEAT CCD is a commercial off-the-shelf part manufactured by Lockheed-Martin Fairchild Systems of Milpitas, CA. It features good cosmetic quality and low dark current. The imaging area is  $4080 \times 4080$  contiguous pixels with less than 0.3% unusable area due to blemishes. There are four output nodes or amplifiers that can be sampled in parallel, one for each  $2048 \times 2048$  pixel quadrant. The read noise is 15 electrons at a readout speed of about 200 kpixels  $\text{s}^{-1}$ . The bandpass is about  $4\text{--}8000 \text{ \AA}$  determined solely by the CCD response (i.e., no filters).

The dewar is aluminum and accommodates the CCD and associated electronics without room to spare. It is filled with dry N gas and sealed before use. Thermal modeling showed no cooling improvement in evacuating this dewar.

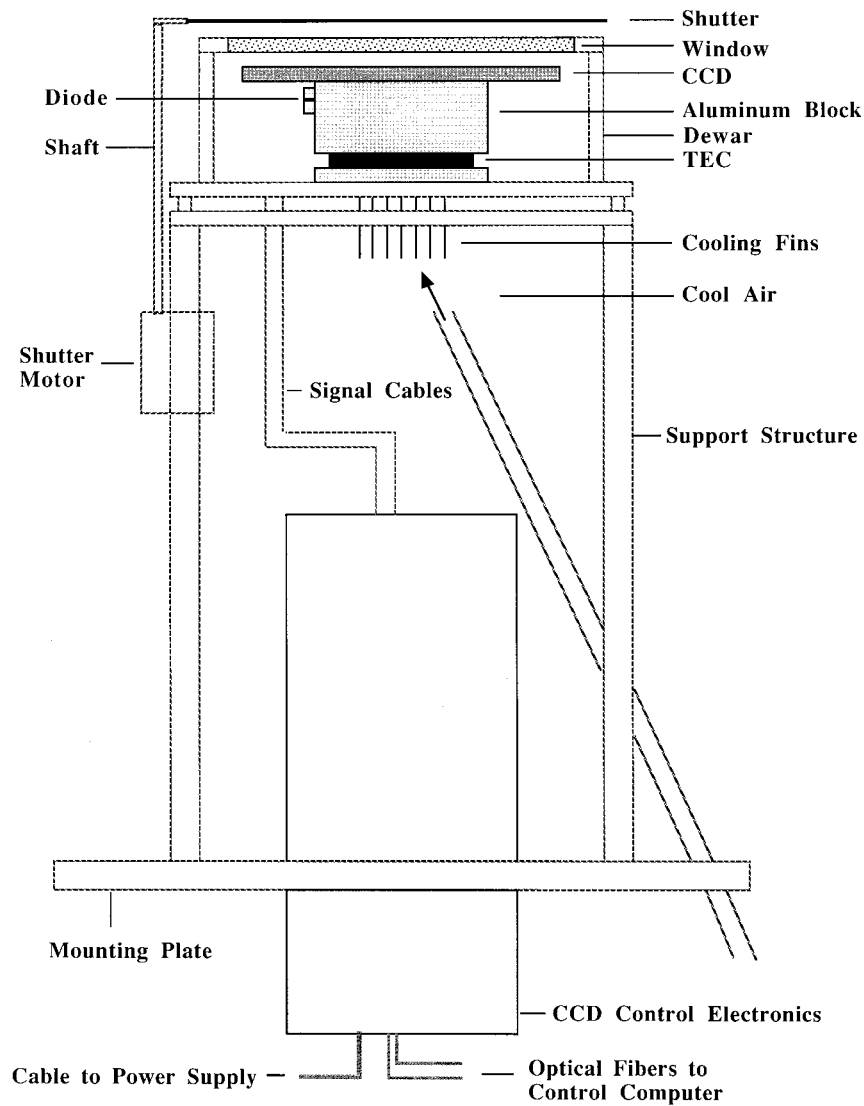


FIG. 2.—Schematic diagram of NEAT camera

A two-stage thermoelectric cooler (TEC), with its cold side in thermal contact with the substrate of the CCD, actively transfers heat from the CCD to the back side of the dewar through an aluminum block acting as a conducting path. A cool air loop then removes the heat from the back side of the dewar. This arrangement maintains the CCD operating temperature within  $\pm 3$  degrees of  $0^\circ\text{C}$ . The temperature is determined from the voltage across a diode in thermal contact with the CCD support. With the diode conducting a small fixed current, the temperature is proportional to the voltage drop. With the CCD kept at  $0^\circ\text{C}$ , the dark current is about  $90\text{ }e^- \text{ s}^{-1} \text{ pixel}^{-1}$ .

The mechanical shutter was built at JPL and has a very low (2 mm), narrow (10 cm) profile to fit into the available space inside the GEODSS telescope. It consists of a metallic blade that rotates into or out of the field of view under motor control in about 0.1 s. Shutter position is commanded by the computer through the camera electronics boards, which provide switching signals to an electronic circuit controlling the shutter motor.

San Diego State University (SDSU) built the camera electronics (Leach 1996). This control system allows software modification of the operating parameters and thus can drive

a variety of CCDs with minor hardware changes. Since NEAT's inception, an earlier CCD with  $2048 \times 2048$  pixels has been replaced with the present CCD and earlier versions of the control electronics have been upgraded to increase the readout speed by a factor of 4 from 50 to 200  $\text{kpixels s}^{-1}$ .

The electronics controlling the CCD consist of four circuit boards: a "timing" board to control the phase and duration of the signals that drive the parallel and serial transfer of charge across the CCD; a "utility" board to control the shutter position and to sample the voltage across the temperature-sensing diode; and two "clock/video" boards, which drive the voltages for the parallel and serial clocks and also sample and digitize the video return signals at the four quadrants of the CCD.

Both the timing and utility boards have their own digital logic that are separately programmable and addressable via an optical fiber link on the timing board. Precompiled Motorola machine code is thereby downloaded from the workstation computer to control the clocking waveform, shutter timing, and readout timing of the CCD. Upon receiving a signal to expose and readout the CCD camera, the timing board returns the digitized signal to the workstation

as a multiplexed, serial byte stream through a separate return fiber.

## 2.2. Computers

The main, on-site controlling computer is a Sun Sparc 20 computer with two central processing units (CPUs) clocked at 75 MHz. Appendix A gives details of the operating system software. Until May of 1998, this one computer not only controlled the telescope and CCD camera, but also ran the software to identify asteroids. With recent upgrades to increase the camera readout speed and to improve the rate of sky coverage, a Sun Enterprise 450 with four CPUs, each clocked at 300 MHz, was added to run the search software.

The Sparc 20 is equipped with electronics built by SDSU to allow the computer to communicate with the camera via the fiber optic link. The components are mounted on a single circuit board that connects directly to Sun's proprietary data bus (SBUS), internal to the Sparc computer. Software to control this SBUS card under the UNIX operating system was cooperatively written by JPL and SDSU engineers, and recently modified at JPL to allow software handshakes between the camera and Sparc 20 during image readout. The same code has successfully operated on other Sun computers, including Sparc 5 and Ultra 2's. The Sparc 20 is also equipped with a commercially available SBUS card (a DR-11 W emulator built by Ikon Corporation) to allow 16-bit parallel communication with the electronics controlling the drive motors of the GEODSS telescope and dome. The telescope communication link runs from the DR-11 W card through two multipin cables to a Binary Interface Unit, part of the GEODSS control system, and from there to the telescope tower using the existing GEODSS connections. The camera communication link is two  $\sim 100$  m long optical fibers from the SDSU SBUS card to the telescope tower. Additional computer peripherals consist of: a Datum Global Positioning System (GPS) receiver (provided by the USAF) to synchronize the internal clock of the Sparc 20 to Universal Time with an accuracy of a few milliseconds using signals from the GPS; approximately 60 Gbytes of hard disk storage; and a 28.8 Kbps modem for transferring data to computers at JPL and for remote monitoring and control of the telescope and camera from JPL. A standard Sun monitor is provided for on-site operators to monitor image quality and system status.

The recently added Enterprise 450 is equipped with 95 Gbytes of disk space. It runs software (described in Appendix B) to search four image triplets in parallel for moving objects, running an identical version of the software on each of its four CPUs and with each CPU assigned to analyze a different triplet. At the current rate of 45 s per image (20 s exposure plus 25 s overhead), this computer is able to keep pace with the acquisition of data. Within minutes of the acquisition of the third image in a triplet, the search of that triplet is completed.

## 2.3. Noise Performance

The sources of noise in the images were determined from analysis of dark and sky frames with varying exposure times. The results show a dark current of 90 electrons  $\text{pixel}^{-1} \text{s}^{-1}$  and a sky brightness of 69 electrons  $\text{pixel}^{-1} \text{s}^{-1}$ . The read noise is about 15 electrons. The cooling is most efficient near the center of the chip and the thermal gradient results in higher dark current by about  $\frac{2}{3}$  toward the edges.

Dark frame subtraction and local flat fielding are needed to enhance object detection over the entire frame.

## 3. OPERATING PROCEDURES

### 3.1. Observing Modes and Planning

The "survey" is the primary NEAT observing mode. It is designed to discover new objects. In preparation for a night of observing, the first task is to create an observing script that lists the position of the search field. For this purpose we use a sequencing program, run once at the start of each six-night run. Figure 3 shows a hypothetical six-night search pattern planned for 1998 September 14–19. The program takes into account the time to expose and read out each image, as well as the number of nights per run and their duration. It thereby determines a search pattern that will uniformly sample the areas of the sky close to the ecliptic and to opposition. In order to keep the telescope pointed near to the meridian, the program targets a given night's search along strips of sky, each perpendicular to the ecliptic, and separated in longitude from one another by  $11^{\circ}25'$ . With the length of a given strip chosen so that it can be searched in  $\sim 45$  minutes ( $\sim 20$  fields for the current NEAT system), the search is completed by the time the next strip approaches the meridian. By shifting the longitude of the search strips each night by  $2^{\circ}25'$ , the program creates a search pattern that uniformly samples the ecliptic within  $45^{\circ}$  of opposition after five nights. Search areas covered on the first night are repeated on the sixth, thus yielding positions with 6 day separation for any objects moving slowly enough ( $\lesssim 0.2 \text{ day}^{-1}$ ) to be detected on both nights.

There are additional constraints that shape the search pattern. We generally choose longer search strips within  $15^{\circ}$  of opposition in order to increase the coverage there. The latitude of the observatory,  $20^{\circ}7' \text{ N}$ , and design of the telescope limit the available declinations to more than  $-38^{\circ}$ . The time of year limits the hour angles between about 3 hr west at astronomical twilight and 3 hr east at astronomical

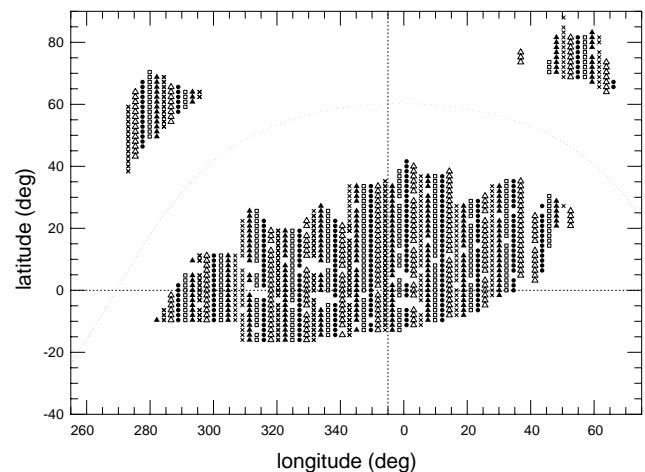


FIG. 3.—Search pattern planned for 1998 September 14–19. Crosses show areas to be searched on the first and sixth night. Open triangles, filled circles, open boxes, and filled triangles show areas to be searched on nights 2, 3, 4, and 5, respectively. The large gaps in the coverage are due to the Galactic plane. Smaller gaps are Spacewatch regions that NEAT cooperatively avoids. The Galactic plane, an area of avoidance for NEAT observations, is shown as a dotted line.

dawn. Observations within  $10^\circ$  of the Galactic plane are also avoided because confusion with stars thwarts asteroid detection. Finally, in cooperation with the Spacewatch search (Scotti, Gehrels, & Rabinowitz 1991), we avoid the relatively small areas of sky that they search each month. The search pattern in Figure 3 shows large gaps where Galactic plane appears, and small holes closer to opposition revealing the typical areas searched by Spacewatch.

In addition to the survey search positions, a few positions are scripted each night to follow-up objects discovered on previous nights or lunations. Weather and schedule permitting, NEAT follows up all candidate NEOs, comets, or other bodies with unusual orbits or properties. Criteria for deciding if an object is worthy of follow-up are described below (§ 3.3). It is also possible to insert new positions into the observing script while the night-time observations are in progress, thus permitting follow-up observations in near real time. Several recently occurring gamma-ray burst fields have also been observed using this near real-time method.

For each target position, the observing script also may be used to specify the observation time to  $\sim 10$  s precision. This feature has been used to test the capabilities of the NEAT system for tracking artificial satellites. Because of the high rates of motion for these objects, the exposures must be obtained within 1 minute of the time they reach their scripted positions. The script may also be used to specify image binning (the summing of neighboring pixels in both the horizontal and vertical directions as an image is read out). Binning reduces the time to read the image in proportion to the number of pixels summed. During tests of satellite tracking, this option has also been used to increase the observation rate.

### 3.2. Observing

Once the observing script has been loaded, and just before the end of nautical twilight, on-site operators prepare the telescope for operation. They remove the mirror cover, open the dome, clear the previous night's data from the disks of the control and analysis computers, and start the control program. The program takes over, pointing the telescope and acquiring images as scripted. The program also acquires dark-current images at 1 hr intervals, taken with the shutter closed but with the same exposure time used for the search images. The search program that runs on the analysis computer subtracts these dark-current images from each sky image as part of the analysis procedure (discussed below). If bad weather interrupts the observing, the operators can pause the control program until the weather clears. It will continue where it left off. After a pause or for any other reason, the program will skip a scripted exposure if there is not enough time to obtain an entire triplet of images before the target position has set below  $10^\circ$  elevation. The control program will proceed with the next position on the script until there are no more, or until the operators stop the program at the start of nautical dawn.

While the control computer executes the observing script, an auxiliary program ("the analysis manager") runs on the analysis computer, monitoring log files generated by the control program. As soon as the control program has acquired a complete triplet of images, the analysis manager adds their file names to a processing queue. Appendix A gives a more complete description of the operations system. For each triplet in the queue, the analysis manager launches an additional program (described in Appendix B) to search

for asteroids and to record their magnitudes and astrometric positions. Up to four instances of this search program can be run in parallel, each using one of the four CPUs of the analysis computer, and each analyzing a different triplet. For each asteroid, the search program also records nine small subarrays or "patches" of image data (about  $25 \times 25$  pixels each), three from each image in the triplet. Of the three patches taken from a given image, one is centered on the measured position for the asteroid, while the other two are centered on the positions where the asteroid appears in the other two images of the triplet. The nine patches are later examined by eye to validate the detection (see discussion below).

### 3.3. Screening

For each analyzed triplet, the search program typically records 50 Kbytes of data (patches plus positions and magnitudes). A typical 10 hr night may yield  $\sim 270$  triplets, or 15 Mbytes of information. This compares with 26 GB of raw image data and corresponds to a data "compression" by the processing system of a factor of  $\sim 2000$ . The processed data are further compressed and transmitted via modem and commercial phone line to JPL as soon as night-time observations are completed. At JPL, team members use a screening program called PATCHVIEW to visually inspect the nine patches associated with each asteroid and also to check the consistency of the measured positions. This serves as a final check of validity of each detection and a way to pick out especially interesting objects for follow-up. Such objects are immediately reported to the worldwide observing community via the Minor Planet Center (MPC).

Figure 4 (*upper*) shows an example of the PATCHVIEW display for a given asteroid. The nine patches are displayed as a  $3 \times 3$  matrix. Column 1 (*left*) shows the three patches from the first exposure. Columns 2 and 3 (*middle and right*) show the three patches from the second and third exposures, respectively. If the asteroid is a valid detection, it should appear centered only within the diagonal patches running from the upper left (row 1, column 1) to the lower right (row 3, column 3). These are the locations where the search program found the asteroid in exposures 1, 2, and 3, respectively. The asteroid should not appear centered in any other patch in the matrix. These "veto" patches show the same locations as the diagonal patches, but at the times when the asteroid had not yet moved there, or when the asteroid had already moved away. For example, columns 2 and 3 of row 1 are patches from images 2 and 3, respectively, showing where the asteroid had appeared in exposure 1. Similarly, columns 1 and 2 of row 3 are patches from exposures 1 and 2 showing where the asteroid would appear in exposure 3.

Visual examination of these nine patches is an efficient method to quickly identify the most common source of false positives from the search program: faint stars at the limit of detection. An example is shown in Figure 4 (*lower*). An object appears centered in the diagonal patches, but also in the veto patches. This observation clearly shows a star, and not an asteroid. The software incorrectly finds an asteroid, here, because it has only marginally detected the star. Because of the influence of random noise, and variation in atmospheric conditions (seeing and extinction), a faint star can appear above the detection threshold in one exposure, but below the threshold in the other two. The search

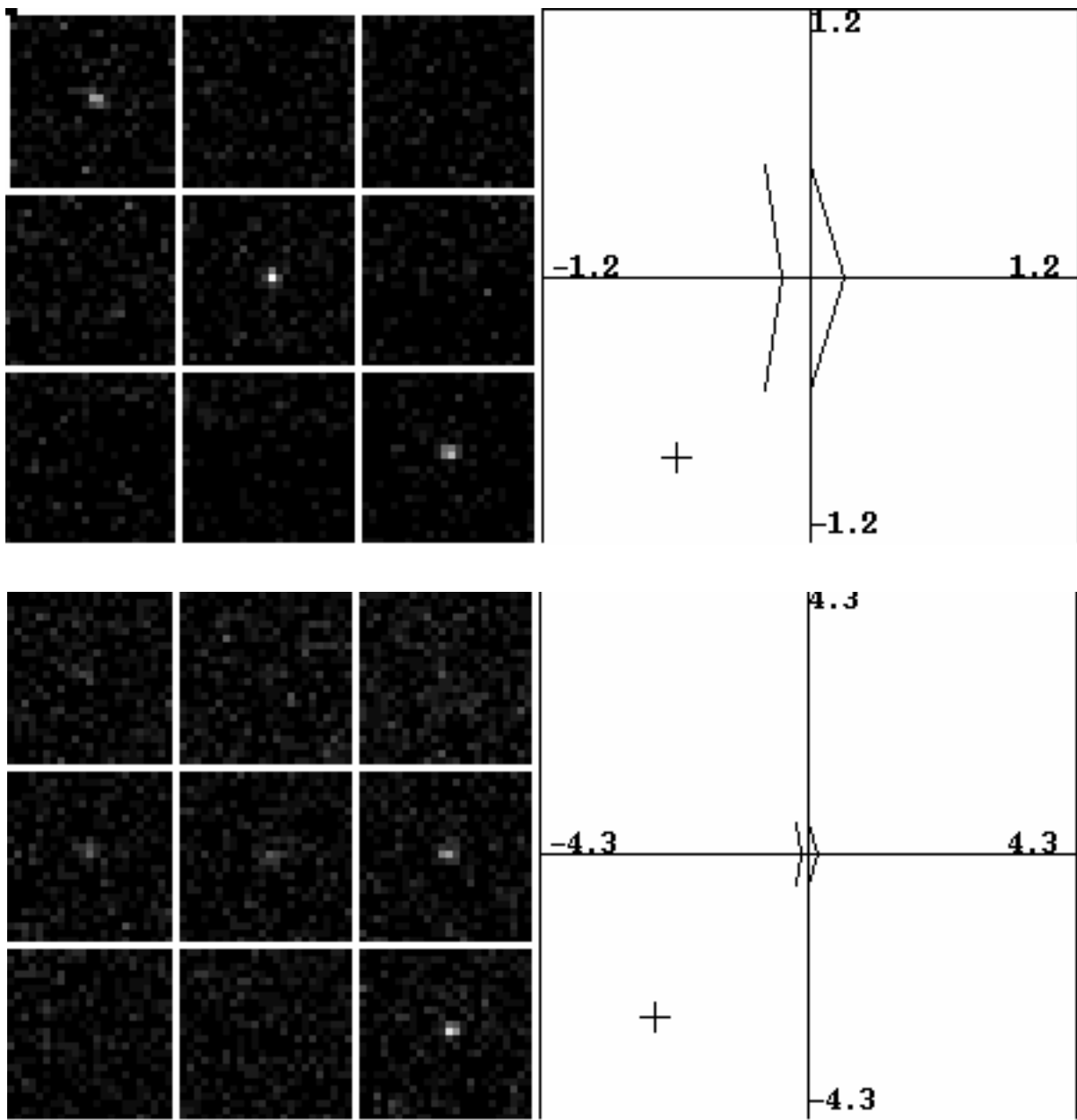


FIG. 4.—PATCHVIEW displays of the discovery image of 1998 DG<sub>16</sub>, an Aten Earth-crossing asteroid (*top*). PATCHVIEW display of a false positive (*bottom*).

program occasionally detects these faint stars (and other image artifacts) in such a way that they appear to be observations of a moving object.

For each asteroid, the PATCHVIEW program also displays ancillary information, such as the time, magnitude, position, and rate of motion (ecliptic and equatorial coordinates). A plot of the ecliptic rate of motion is used to decide if the asteroid has an interesting rate of motion. If the motion is outside the boundaries for the motion expected of main-belt asteroids (empirically determined, see Rabinowitz 1991), it is scheduled for follow-up and reported to the MPC as an interesting object. PATCHVIEW also calculates the deviation of each asteroid's measured positions from linear motion. If the deviation is larger than would be expected from measurement error, a decision may be made to reject the object, or to make further confirmatory observations before reporting it.

Each object detected with NEAT is assigned a unique, unpronounceable name. First a number is constructed based on the elapsed time of an exposure starting with the beginning of 1995, incremented by the object number within the exposure. This number is then translated into a six-alphanumeric character name. Base 36 (26 letters and 10 digits) is used. The largest number is therefore  $36^6 = 2,176,782,336$ . For 10 yr of observations with one exposure every 10 s this allows 70 unique names for objects per exposure. When an object is confirmed by recovery on a subsequent day with NEAT or other observers, it is assigned an official preliminary designation by the MPC.<sup>4</sup>

<sup>4</sup> Daily updates of NEAT results during operational periods can be accessed via the World Wide Web at address <http://huey.jpl.nasa.gov/~spravdo/neat.html>

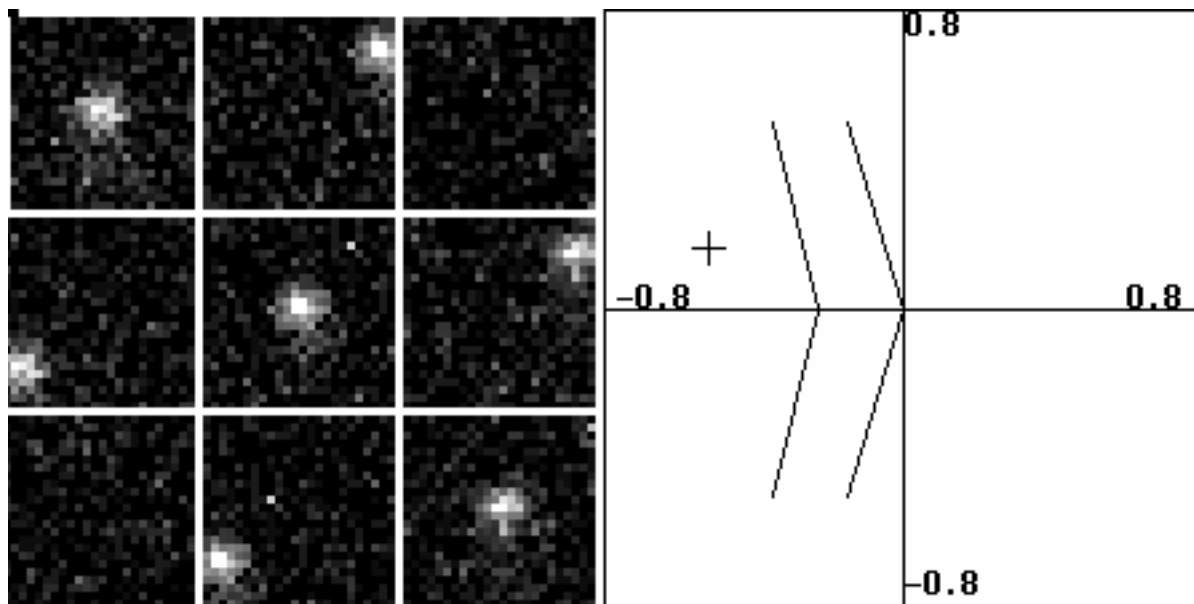


FIG. 5.—PATCHVIEW discovery image of Comet 1997A1

### 3.4. Archiving

At the end of the evening, while the night's haul of data is downloaded and screened at JPL, an archive program (M. Klimesh 1998, private communication) is run remotely at the Maui site to compress all the raw image data collected during the night (lossless compression by a factor  $\sim 2$ ) and store it to Digital Linear Tape (using a Quantum DLT7000 tape drive). These tapes are later shipped to JPL for incorporation into the *SkyMorph* archive (Pravdo et al. 1998). This is a separate research program cooperatively run by JPL and NASA Goddard Space Flight Center. The goal is to create a database of images and object information (brightness, shape, and position versus time for asteroids, comets, stars, galaxies, etc.) derived from the NEAT data and accessible on the internet. To date, more than 25,000 NEAT images have been archived by the *SkyMorph* project.<sup>5</sup>

## 4. RESULTS

### 4.1. Discoveries and Incidental Detections

Since December of 1995, NEAT has detected more than 26,400 asteroids, and been credited with discovery of 32 NEAs, two comets (C/1996 E1 and C/1997 A1), and the only known asteroid (1996 PW) with an orbit indistinguishable from an Oort-cloud comet (Rabinowitz et al. 1996; Weissman & Levison 1997; Hicks et al. 1998; Davies et al. 1998). Table 1 lists the orbital elements calculated by the MPC ( $a$  is the semimajor axis,  $q$  is the perihelion,  $e$  is the eccentricity,  $i$  is the inclination) not only for NEAs discovered by NEAT, but also for previously discovered NEAs that were detected solely by chance (incidental detections). The table is sorted by absolute magnitude,  $H$ , rounded by the MPC to the nearest 0.5 mag. All detections were flagged as interesting by our screening program (described in § 3.3). For each NEA, the table also lists the observed visual mag-

nitude,  $V$ , and opposition geometry (longitude with respect to opposition,  $d_{\text{lon}}$ , and latitude,  $lat$ ) and the angular rate,  $w$ , at detection.

Tables 2 and 3 show the orbital elements for the comets and unusual minor planets discovered with NEAT, respectively. NEAT has serendipitously detected four comets in addition to its two discoveries (see Fig. 5). Unusual minor planets such as 1996 PW are not NEAs but are notable since they have eccentricities ( $e$  in Table 3) larger than 0.4.

### 4.2. Limiting Magnitude

To evaluate the effective limiting magnitude,  $V_L$ , for asteroid detection, we show in Figure 6 the number of detected asteroids,  $N$ , as a function of apparent magnitude,  $V$ . Nearly all of these asteroids are in the main belt. Each observation was verified by visual inspection (see § 3.3) and reported to the MPC during the course of normal survey operations during the period 1995 December to August 1998. As discussed in Rabinowitz (1993), there is a turnover

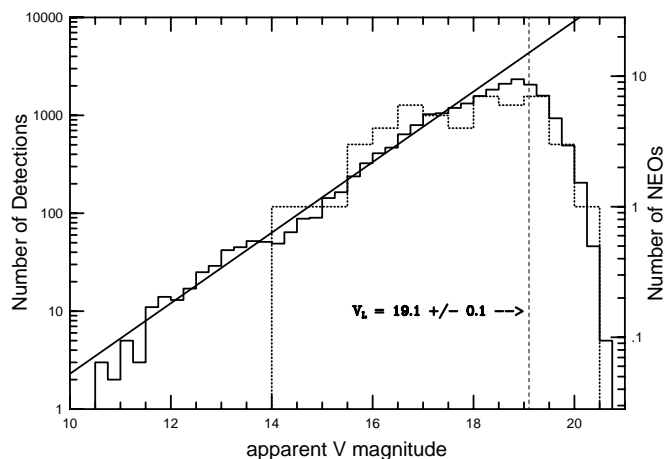


FIG. 6.—Number of detected asteroids (solid line) and number of detected NEAs (dotted line) vs. apparent  $V$  magnitude. The heavy line is a linear fit to the distribution from  $V = 12$ –18. Limiting magnitude,  $V_L$ , occurs where the observed distribution deviates from the linear fit by 0.5.

<sup>5</sup> The archive can be accessed via the World Wide Web at address <http://skys.gsfc.nasa.gov/skymorph/skymorph.html>

TABLE 1  
ORBITAL ELEMENTS AND DISCOVERY CIRCUMSTANCES FOR DETECTED NEAR-EARTH ASTEROIDS

Designation	<i>a</i> (AU)	<i>q</i> (AU)	<i>e</i>	<i>i</i> (deg)	<i>H</i>	dlon (deg)	lat (deg)	<i>w</i> (deg day <sup>-1</sup> )	<i>V</i>	MJD – 50,000	Class
1917 .....	2.15	1.066	0.504	23.9	13.9	–16.4	–3.0	0.3	19.2	543	Amor
1980 .....	1.71	1.086	0.365	26.9	13.9	–57.7	–13.4	0.6	14.7	812	Amor
4183 .....	1.98	0.717	0.638	6.8	14.4	–1.4	12.3	0.5	17.0	751	Apollo
5626 .....	2.196	1.201	0.453	3.9	14.7	–73.6	0.0	0.4	16.0	372	Amor
5751 .....	2.104	1.214	0.423	16.1	14.8	–69	–13.4	0.5	16.3	838	Amor
1997 SE <sub>5</sub> * .....	3.722	1.239	0.667	2.6	15.0	–62.2	6.9	0.9	15.4	719	Amor
2368 .....	2.105	1.234	0.414	5.3	15.2	16.1	–2.4	0.3	20.2	463	Amor
4179 .....	2.512	0.919	0.634	0.5	15.3	–25.6	–0.2	0.5	15.7	312	Apollo
7889 .....	1.261	0.825	0.346	36.9	15.3	–36.8	45.8	0.8	17.8	989	Apollo
5653 .....	1.794	1.249	0.304	6.9	15.4	16.7	–10.2	0.4	17.6	934	Amor
1997 WU <sub>22</sub> * .....	1.468	0.819	0.442	16	15.5	–1.3	7.4	0.5	18.7	782	Apollo
3838 .....	1.505	0.448	0.702	29.3	15.5	–93.6	2.6	1.1	18.5	812	Apollo
1998 FM <sub>5</sub> * .....	2.265	1.008	0.555	11.5	16.0	–67.8	–5.2	2.0	15.6	896	Amor
1998 OH* .....	1.542	0.914	0.407	24.5	16.0	–29.1	56.6	0.4	18.1	1013	Apollo
1862 .....	1.471	0.647	0.560	6.4	16.2	–51.8	3.2	0.8	16.8	935	Apollo
1996 EN* .....	1.507	0.857	0.431	38	16.5	–24.8	0.5	0.9	16.4	157	Apollo
1996 TO <sub>5</sub> * .....	2.381	1.152	0.516	21	16.5	–64.5	–0.7	0.4	19.0	365	Amor
1997 TD* .....	2.25	1.197	0.468	12.9	16.5	–72.6	–14.4	0.9	17.0	722	Amor
1998 BX <sub>7</sub> * .....	2.609	1.294	0.504	9	16.5	20.9	–4.2	0.4	18.2	837	Amor
1998 EC <sub>3</sub> .....	2.131	1.038	0.513	8.4	16.5	–41.9	12.4	0.4	19.8	873	Amor
1998 OR <sub>2</sub> * .....	2.361	1.025	0.566	5.9	16.5	16.5	–11.8	0.4	19.2	1018	Amor
7482 .....	1.346	0.905	0.328	33.5	16.8	7.6	–16.1	2.9	17.3	315	Apollo
1996 FR <sub>3</sub> * .....	2.165	0.444	0.795	8.3	17.0	24.4	4.3	0.8	16.6	168	Apollo
1996 SK* .....	2.428	0.495	0.796	2	17.0	–9.5	2.0	0.6	19.5	343	Apollo
1997 GH <sub>3</sub> * .....	2.487	1.062	0.573	3	17.0	–80.2	–1.2	1.5	16.7	544	Amor
1998 BZ <sub>7</sub> * .....	2.038	0.907	0.555	6.5	17.5	30.8	8.8	0.6	17.2	837	Apollo
1998 BP <sub>26</sub> * .....	1.719	1.279	0.256	20.2	17.5	58.2	5.7	0.8	18.2	841	Amor
1994 CK <sub>1</sub> .....	1.901	0.698	0.633	4.6	17.5	–57.2	–15.8	1.0	17.2	988	Apollo
1997 NC <sub>1</sub> * .....	0.866	0.685	0.209	16.7	18.5	–83.5	–0.3	2.4	16.5	634	Aten
1998 FX <sub>2</sub> .....	2.149	1.087	0.494	10	18.5	–8.7	2.8	2.2	14.2	894	Amor
1998 FX <sub>134</sub> .....	2.262	1.294	0.428	5.2	18.5	–9	3.8	0.2	18.6	892	Amor
1996 EO* .....	1.341	0.803	0.401	21.6	19.0	6.6	0.1	1.2	16.9	157	Apollo
1996 KE* .....	2.565	1.188	0.537	24.3	19.0	–16.3	2.1	2.2	15.8	222	Amor
1996 TE <sub>9</sub> * .....	1.793	1.208	0.326	21.6	19.0	–32.6	–0.3	1.6	18.0	369	Amor
1997 UH <sub>9</sub> * .....	0.83	0.436	0.475	25.5	19.0	20.4	–6.1	2.0	17.6	750	Aten
1998 FF <sub>2</sub> .....	1.562	1.106	0.292	11	19.0	–9.8	2.8	0.6	19.7	892	Amor
1998 BG <sub>9</sub> * .....	2.507	1.168	0.534	13	19.5	31.5	16.9	1.1	18.1	837	Amor
1997 PN* .....	2.224	1.285	0.422	26.4	20.0	–4.6	–3.7	1.7	18.5	661	Amor
1997 WB <sub>21</sub> * .....	1.461	0.996	0.318	3.4	20.5	–40.1	15.4	1.4	18.8	778	Apollo
1997 YR <sub>10</sub> * .....	1.721	1.146	0.334	36.8	20.5	–32.6	–10.1	3.2	18.5	811	Amor
1998 BB <sub>10</sub> * .....	1.274	0.731	0.426	11.6	20.5	11	3.2	1.5	17.8	838	Apollo
1998 DG <sub>16</sub> * .....	0.902	0.593	0.343	15.7	20.5	39.9	–3.2	1.0	19.0	871	Aten
1996 FQ <sub>3</sub> * .....	2.031	1.074	0.471	1.1	21.0	23.4	4.8	1.0	17.2	168	Amor
1996 RY <sub>3</sub> * .....	1.211	1.043	0.139	37.4	21.0	6.7	2.0	2.6	18.7	341	Amor
1997 AC <sub>11</sub> * .....	0.913	0.577	0.368	31.7	21.0	43.8	–2.8	2.3	19.0	458	Aten
1998 HD <sub>14</sub> * .....	0.964	0.662	0.313	7.8	21.0	–27.4	41.2	1.1	19.1	928	Aten
1998 HT <sub>31</sub> * .....	2.533	0.770	0.696	6.8	21.0	2.2	6.9	1.8	16.6	932	Apollo
1996 TD <sub>9</sub> * .....	1.333	0.794	0.404	5	24.0	12.1	7.4	2.1	19.9	368	Apollo
1997 YM <sub>9</sub> * .....	1.095	0.981	0.104	7.9	25.0	31.8	10.6	4.2	18.8	810	Apollo

NOTE.—NEAT discoveries are marked by asterisks.

at the faint end of the histogram, where the efficiency of detection decreases. Limit  $V_l$  is the value of  $V$  for which the efficiency drops by 50% relative to the nominal efficiency at bright magnitudes (discussed further, below). This limit is found by fitting a function of the form  $f(V) = 10^{[c_1 + c_2 V]}$  to  $N(V)$  at bright magnitudes ( $V = 12$  to  $18$ ) and evaluating the expression  $N(V_l)/f(V) = 0.5$ . With  $c_1 = -3.241 \pm 0.069$  and  $c_2 = 0.3602$ , this yields  $V_l = 19.1 \pm 0.1$ . Here we estimate the error in  $V_l$  from the uncertainty of our magnitude calibrations ( $\pm 0.1$  from observation of faint standards) and from the uncertainty in  $c_1$ .

Note that the value we determine for slope  $c_2$  is lower by  $\sim 20\%$  than the slope reported by Rabinowitz (1993) for Spacewatch observations of main-belt asteroids. This variance may result from two important differences between NEAT and Spacewatch: (1) NEAT does not detect the slower main-belt asteroids with  $w < 0.15 \text{ day}^{-1}$ , whereas the Spacewatch cutoff is  $w \lesssim 0.05 \text{ day}^{-1}$  (Rabinowitz 1994); and (2) the NEAT efficiency for detection of main-belt asteroids does not vary significantly with  $V$  for  $V < 18$  (see discussion below), whereas the Spacewatch efficiency drops from 80%–90% for  $V > 19$  to  $\sim 60\%$  for  $V = 14$ – $19$ .



TABLE 2  
COMETS DETECTED WITH NEAT

Name	Period (yr)	$i$ (deg)	$q$ (AU)	$w$ (deg day <sup>-1</sup> )
1996 E1* .....	Parabolic	114.4	1.35	0.9
1997 A1* .....	Parabolic	145.0	3.16	0.6
128P-B .....	9.51	4.4	3.05	0.2
69P .....	6.97	20.5	1.95	0.3
21P .....	6.61	31.9	1.03	0.3
1998 M2 .....	Parabolic	60.2	2.73	0.3

NOTE.—NEAT discoveries are marked by asterisks.

(Jedicke & Herron 1997). Difference (1) prevents NEAT from detecting as large a fraction of distant asteroids at the outer edge of the main-belt as Spacewatch, thereby lowering the relative number of faint detections. Difference (2) artificially biases Spacewatch against the detection of bright asteroids, thereby increasing the slope of their magnitude-frequency curve relative to NEAT. A more detailed analysis of these effects will be required to fully understand the different values observed for the slope and will be reported elsewhere. However, it is clear from the results of Spacewatch that the magnitude-frequency of the main-belt asteroids does not decrease in the range  $V = 18$  to 20. Hence, the decrease observed by NEAT in this range must be a measure of the decrease in detection efficiency.

Also plotted in Figure 6 are the number of detected NEAs versus  $V$ . If there were more detections, we could separately determine  $V_l$  for these objects from the shape of their magnitude-frequency curve. Given the limited number, however, it is more accurate to use the main-belt curve. It is nonetheless clear from Figure 6 that the limiting magnitude determined from the main-belt detections is consistent with the limit for NEA detections.

Note that this limiting magnitude is averaged over the field. The limiting magnitude at the center of the field is fainter than this average and the limiting magnitude at the edges of the field is brighter due to optical aberrations and lower cooling efficiency. To estimate this variation we summed the number of detections over a representative time interval along rows and columns and examined the relative detection efficiency. The efficiency varied by  $\pm 25\%$  relative to the mean. Since  $N(V)$  varies as  $10^{[3.241 + 0.3602V]}$ , a 25% variation corresponds to a 0.26 change in the magnitude limit. The limiting magnitude is thus 0.26 mag fainter at the center of the CCD, and 0.25 mag brighter at the edges. It varies smoothly in between.

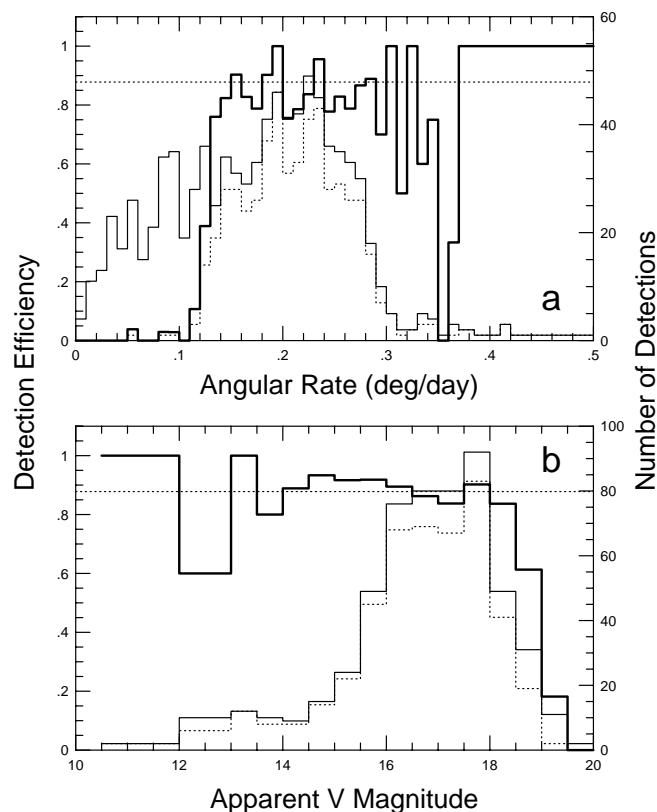


FIG. 7.—Detection efficiency (heavy solid line), number of expected detections of numbered asteroids (light solid line) and number of detected numbered asteroids (dotted line) as a function of (a) of apparent angular rate and (b) of apparent  $V$  magnitude but only numbered asteroids with  $w > 0.15$  day<sup>-1</sup>

#### 4.3. Absolute Detection Efficiency

To evaluate the absolute efficiency of the NEAT system, we calculated the expected positions and  $V$  magnitudes of all numbered asteroids appearing in our search fields in selected clear nights (December 25 in 1997, January 24, February 23, February 25, March 24, and March 25 in 1998). Orbital elements and  $H$ -values were taken from the MPC catalog. For each predicted position, a check was made for a detected asteroid with consistent position, rate, and magnitude. Figure 7a shows the expected number, the detected number, and the fractional number detected (detection efficiency) as a function of  $w$ . It is apparent that our efficiency is nearly constant (to within sampling error)

TABLE 3  
UNUSUAL MINOR PLANETS DISCOVERED WITH NEAT

Name	$a$ (AU)	$q$ (AU)	$e$	$i$ (deg)	$P$ (yr)	$D$ (km)	$w$ (deg day <sup>-1</sup> )
1996 PW .....	327	3.270	0.99	29.8	4900	6.5	0.3
1996 TA <sub>9</sub> .....	2.72	1.360	0.50	12.2	4.74	0.43	0.6
1997 CO <sub>5</sub> .....	2.62	1.362	0.48	18.9	4.25	1.5	0.6
1997 GF <sub>3</sub> .....	3.07	1.781	0.42	42.2	5.50	1.5	0.9
1997 PO .....	3.06	1.744	0.43	23.6	5.97	2.0	0.5
1997 RD <sub>1</sub> .....	2.66	1.596	0.40	13.5	4.45	3.0	0.4
1997 YL <sub>11</sub> .....	2.67	1.549	0.42	36.8	4.38	1.5	0.1
1998 BE <sub>7</sub> .....	3.09	1.514	0.51	14.4	5.12	5.0	0.6
1998 FS <sub>11</sub> .....	2.29	1.351	0.41	4.3	3.46	0.43	0.2

for  $w > 0.15 \text{ day}^{-1}$ . For  $w < 0.11 \text{ day}^{-1}$ , the efficiency is near 0. At such low rates, the pixel displacement of an asteroid is less than can be resolved (3 pixels =  $4''.3$ ) by the NEAT system in the nominal time interval (15 minutes) between search images. Despite the loss of objects moving at slow rates we have maintained our sampling interval at 15 minutes because the number of false detections is dramatically lower than that at longer intervals, decreasing with the square of the interval.

Figure 7b shows the expected and detected number of asteroids and the resulting detection efficiency as a function of  $V$ , but only for numbered asteroids with  $w > 0.15 \text{ day}^{-1}$ . Here,  $V$  is the predicted value for the asteroids, adjusted by  $+0.5 \text{ mag}$  to account for an observed variance between the observed and predicted values. We make this correction because we believe that our measured magnitudes are correct (to within  $\sim 0.1 \text{ mag}$ ), and it is more likely that we have inaccurately predicted the apparent  $V$  magnitudes of the numbered asteroids. Our measured  $V$  magnitudes for NEOs generally agree to within  $\sim 0.1 \text{ mag}$  with those reported by follow-up observers in the Minor Planet Electronic Circulars (A. Harris 1998, private communication). On the other hand, the  $V$  magnitudes of the numbered asteroids cannot be predicted with better than  $0.5 \text{ mag}$  precision because most have unknown spectral albedos, unknown variations of magnitude with solar phase angle, and because their listed values for  $H$  are rounded to the nearest  $0.5 \text{ mag}$ . Averaging the resulting detection efficiency, weighted by the number of detections in each magnitude bin in Figure 7b, yields  $88.0 \pm 0.1\%$  for  $V < 18$ . The efficiency drops to  $50\%$  at  $V \sim 19$ , consistent with the value  $V_i = 19.1$  derived in § 4.2, above. It is not clear why the detection efficiency is not  $100\%$  but reasons include losses due to object confusion, field or quadrant edges, and variable clouds. The NEAT absolute detection efficiency is comparable to the only other published value for an NEO detection system (Jedicke & Herron 1997).

Although the efficiencies plotted in Figures 7a and 7b and the value for  $V_i$  determined in § 4.2 were determined from observations of main-belt asteroids, we expect these results also to apply to the detection of NEAs with higher angular rates. Given our  $20 \text{ s}$  exposures and pixel scale of  $1''.4$ , an object must move more than  $2^\circ \text{ day}^{-1}$  before leaving a trail. Below that rate, the only difference between the detection of a main-belt asteroid and the detection of faster moving objects is the displacement between exposures, which we do not expect to influence detection efficiency. Above  $2^\circ \text{ day}^{-1}$ , image trailing will have some influence on the accuracy of centroid measurements. However, because of tracking errors and focus variation across the field, the trail would have to be longer than 3 pixels before it would have a significant influence. Hence, we expect the detection efficiencies and magnitude limit discussed above to apply to the detection of NEAs with rate of motion as high as  $5^\circ \text{ day}^{-1}$ .

#### 4.4. Sky Coverage

As we have made technical improvements to our system, our rate of sky coverage has increased with time. Since the start of operations with our  $4K \times 4K$  chip in 1996 April, and up until 1997 August, the average time required to complete a single  $20 \text{ s}$  exposure was  $\sim 160 \text{ s}$ . This included  $10\text{--}20 \text{ s}$  to position the telescope,  $\sim 10 \text{ s}$  to clear the CCD image and prepare the camera for the next exposure,  $\sim 80 \text{ s}$

to read out the exposure and download the image to the workstation computer, and  $\sim 20 \text{ s}$  to descramble the multiplexed byte stream from the four quadrants of the CCD image. Overhead to reread failed exposures (caused by intermittent transmission errors) added an additional  $\sim 10 \text{ s}$  per image. In 1997 August, SDSU delivered upgraded control electronics, allowing us to read out our CCD in  $23 \text{ s}$ . We also made various improvements to speed camera preparation and image descrambling and to reduce transmission errors. Our complete cycle time then dropped to  $73 \text{ s}$ . Finally, in 1998 May we modified our control program so that it no longer waited for the read out of an exposure to complete before moving the telescope to the next scripted position. We also off-loaded the descrambling task to the analysis computer. These modifications decreased the cycle time to its current value of  $45 \text{ s}$ .

Figure 8 shows our cumulative sky coverage for the total period of time we have operated with the  $4K \times 4K$  chip. Changes in the slope of the curve occur when changes were made in the cycle time, discussed above, and when the Air Force reduced our time allocation from twelve to six nights (1997 January). Since 1998 June, our rate of sky coverage has been  $\sim 70 \text{ deg}^2 \text{ hr}^{-1}$ , allowing us to search  $700 \text{ deg}^2$  per  $10 \text{ hr}$  night, or approximately  $4200 \text{ deg}^2$  per run of six clear nights. In fact the observing efficiency because of weather is only about  $65\%$  resulting in sky coverage of about  $2700 \text{ deg}^2$  per run. Figure 9 shows 2 years of NEAT sky coverage in celestial coordinates. Note that the ecliptic plane is well-

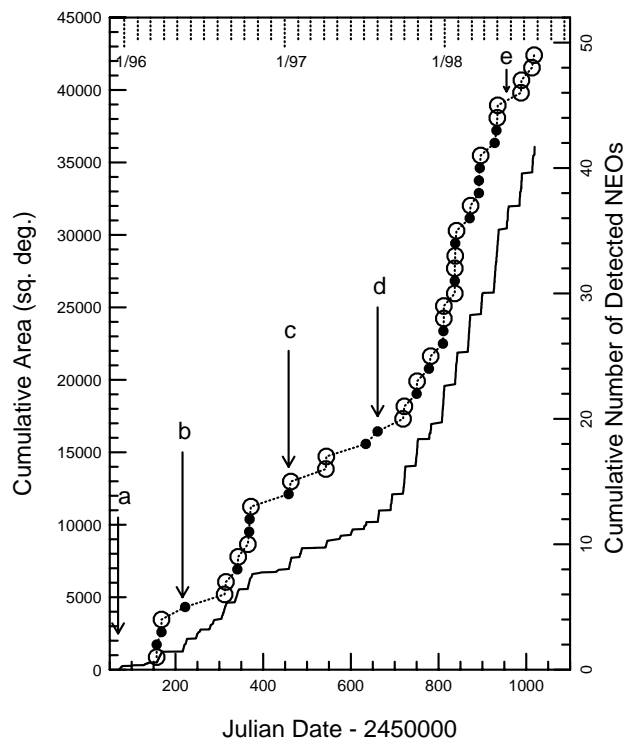


FIG. 8.—Cumulative sky coverage (solid line) and cumulative number of detected NEAs (dotted line) vs Julian date. Large open circles and small filled circles show detections of NEAs larger and smaller than  $1 \text{ km}$  ( $H < 18$  and  $H \geq 18$ ), respectively. Labeled events are (a) NEAT begins, (b)  $4k \times 4k$  CCD replaces  $2k \times 2k$  CCD, (c) number of nights per month's run is decreased from 12 to 6, (d) readout speed is increased from  $50 \text{ kpixels s}^{-1}$  to  $200 \text{ kpixels s}^{-1}$  with the new SDSU electronics, and (e) efficiencies are introduced in camera and telescope operations with the new computer system. A typical sky coverage rate taken from 1998 July is  $73 \text{ deg}^2 \text{ hr}^{-1}$  (each area of the sky covered three times).

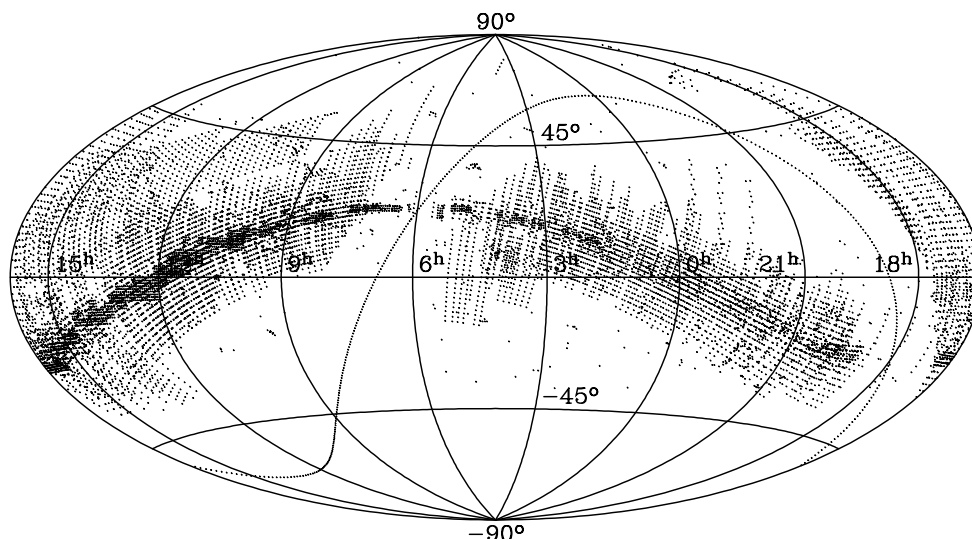


FIG. 9.—Celestial coordinates of areas searched by NEAT 1995 December to 1998 July. The Galactic plane, an area of avoidance for NEAT observations, is shown as a dotted line.

delineated. Gaps in the sky coverage occur where the ecliptic and Galactic planes intersect.

#### 4.5. Rate of Discoveries and Detections

The dotted line in Figure 8 shows the cumulative number of NEAs we have detected (including incidental detections) as a function of time. This curve naturally follows the plot of cumulative search area because the chance of detecting an NEA increases with sky coverage. NEAs with diameters,  $d > 1$  km ( $H < 18$ ), are represented by large unfilled circles. Smaller NEAs are presented by small, filled circles. We have detected a total of 49 NEAs after searching 36,000 deg<sup>2</sup>, thus yielding an average detection rate of  $1.4 \pm 0.2$  NEAs per 1000 deg<sup>2</sup>. Of these detections  $\sim 54\%$  are discoveries, and 58% are NEAs larger than 1 km ( $H < 18$ ). Note that in some cases, our incidental detections would be discoveries had other search programs not been searching the same areas at the same time (e.g., 1998 EC<sub>3</sub>, 1998 FF<sub>2</sub>, 1998 FX<sub>2</sub>, 1998 FX<sub>134</sub>).

#### 4.6. NEA Detection Rate versus Opposition Geometry

As described in § 3.1, our strategy for choosing search areas is to concentrate on the areas close to the ecliptic and to opposition. This maximizes our detection rate for main-belt asteroids, which serve as a good measure for our system performance (see §§ 4.2 and 4.3). This strategy may also enhance our detection rate of NEAs, although by a smaller factor than for main-belt asteroids because the apparent distribution of NEAs on the sky is not as strongly concentrated toward the ecliptic or toward opposition (Drummond & Rabinowitz 1993; Bowell & Muinonen 1994).

Figures 10a and 10b show the total area we have searched (solid line) as a function of  $\sin(\text{lat})$  and  $d_{\text{lon}}$ , respectively. Also shown are the numbers of main-belt asteroids (faint dashed line) and NEAs (heavy dotted line) we have detected as a function of the same two angles. The curves have been scaled to overlap at their peak values (the scale for the main-belt detections is 500 times the scale for the NEAs). If NEAs were preferentially detected close to the ecliptic or

close to opposition, then the number of detected NEAs would drop off more quickly with  $\sin(\text{lat})$  or  $d_{\text{lon}}$  than would the search area.

Comparing the curves for search area, for detected NEAs, and for main-belt asteroids in Figures 10a and 10b, it is clear that the NEAs are not preferentially detected at opposition. As a function of  $d_{\text{lon}}$ , the two curves are similar for

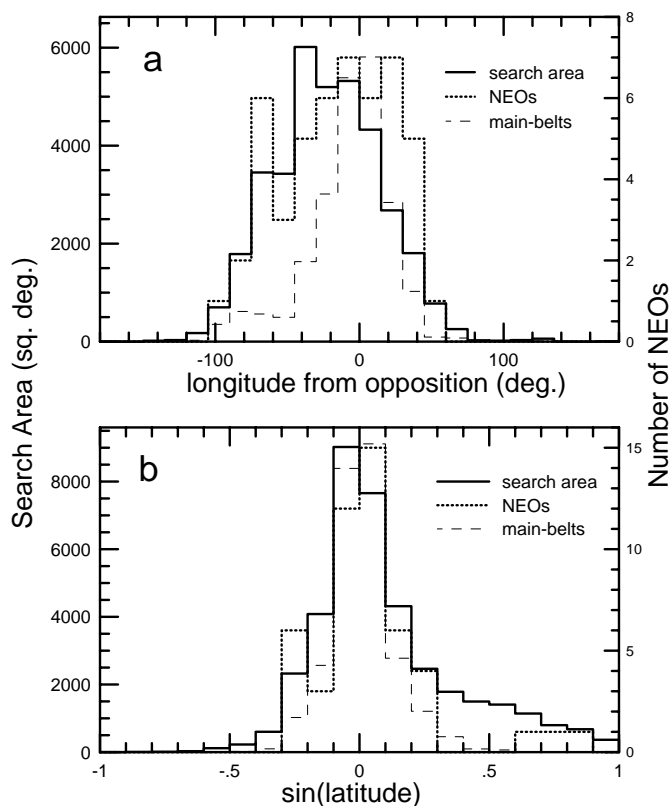


FIG. 10.—Area searched (solid line), number of NEAs detected (dotted line), and number of main-belt asteroids detected (light dashed line) as a functions of (a) longitude from opposition and (b)  $\sin(\text{latitude})$ .

TABLE 4

NUMBER OF NEAs DISCOVERED BY THE MAJOR SEARCH GROUPS:  
1997 OCTOBER 15 TO 1998 AUGUST 8

Objects	NEAT	Spacewatch	LINEAR
Atens .....	3	0	0
Apollos .....	7	17	29
Amors .....	6	7	30
All NEAs .....	16	24	59
All NEAs > 1 km.....	7	4	10
Nights per month.....	6	18	10–18

$d_{\text{lon}} = -120^\circ - 0^\circ$ . For  $d_{\text{lon}} = 0^\circ - 50^\circ$ , the NEA detection drops off less quickly than area. For main-belt detections, however, the drop-off relative to area is pronounced, especially in the range  $d_{\text{lon}} = -50^\circ - 0^\circ$ . As a function of  $\sin(\text{lat})$ , the NEA detections and search area are similar except in the interval  $\sin(\text{lat}) = 0.3 - 0.6$ . Here there are no detected NEAs, although  $4420 \text{ deg}^2$  have been searched. If our detection rate of NEAs were independent of  $\text{lat}$ , we should have detected about six NEAs in this interval. On the other hand, at higher latitudes ( $\sin(\text{lat}) = 0.6 - 0.9$ ) we detect NEAs at approximately the same rate (three detections in  $2430 \text{ deg}^2$ ) as near the ecliptic. This is not the case for the main-belt detections, which clearly drop off more quickly with  $\sin(\text{lat})$  than area, and for which there are no detections for  $\sin(\text{lat}) > 0.6$ .

#### 4.7. Comparisons with Other Search Programs

To compare the performance of the NEAT search with the performance of other search programs, we have examined the orbits and absolute magnitudes,  $H$ , for all NEAs listed by the MPC with discovery dates from 1997 October 15 to the present (1998 August 8). Table 4 shows the total number of bodies of each orbital type (Atens that have semimajor axis,  $a < 1.0 \text{ AU}$ , Apollos that have  $a > 1.0 \text{ AU}$  and perihelion,  $q < 1.0 \text{ AU}$ , and Amors that have  $q < 1.3 \text{ AU}$ ) that have been credited to the three dominant search programs (NEAT, Spacewatch, and LINEAR). Also shown for each group are the total number of discovered NEAs,

the total number with likely diameters greater than  $1 \text{ km}$  ( $H < 18$ ), and the number of nights per month's observing run. The time period is chosen so that it represents an interval when all three programs have been active.

From Table 4 it is apparent that LINEAR and Spacewatch have detected the greatest number of NEAs, respectively 1.5 and 3.7 times the number detected by NEAT. The main reason for this predominance is that LINEAR and Spacewatch have had more frequent telescope time (18 nights per month for Spacewatch, 10–18 nights per month for LINEAR, only six for NEAT). However, for bodies larger than  $1 \text{ km}$ , NEAT's relative detection rate is much higher. Table 4, respectively, shows 7, 4, and 10 detected by NEAT, Spacewatch, and LINEAR. Given the fewer number of observing nights for NEAT, it is apparent that NEAT has had the highest efficiency for detecting the larger NEAs.

#### 4.8. Satellite Tracking

On the night of 1997 November 26 (UT), tests were made of the NEAT capability for satellite tracking. Prior to the start of the night, multiple positions were calculated for 13 different satellites with precisely known orbits and scripted for observations by the NEAT control program. Precise observation times were scripted, so that the target satellites would appear nearly centered in each exposure. Images were binned  $2 \times 2$  pixels to reduce the readout time to 10 s. Also, for each exposure the control program was configured to open the shutter for 10 s, wait with the shutter closed for 10 s, and then open the shutter for an additional 20 s before reading out the image. Owing to the motion of the satellite during the interval with the shutter closed, each satellite left two trails in the image. This allowed for multiple measures of each satellite's position from a single exposure. Figure 11 shows one of the satellite images obtained in this way. Notice that another satellite image was captured on the same field. (The fixed noise pattern in the image is a result of this camera code implementation of  $2 \times 2$  binning.)

Figure 12 shows the difference between the measured and expected positions resulting from the NEAT observations, with the declination residuals plotted against the residuals in right ascension. Because of the precision with which the

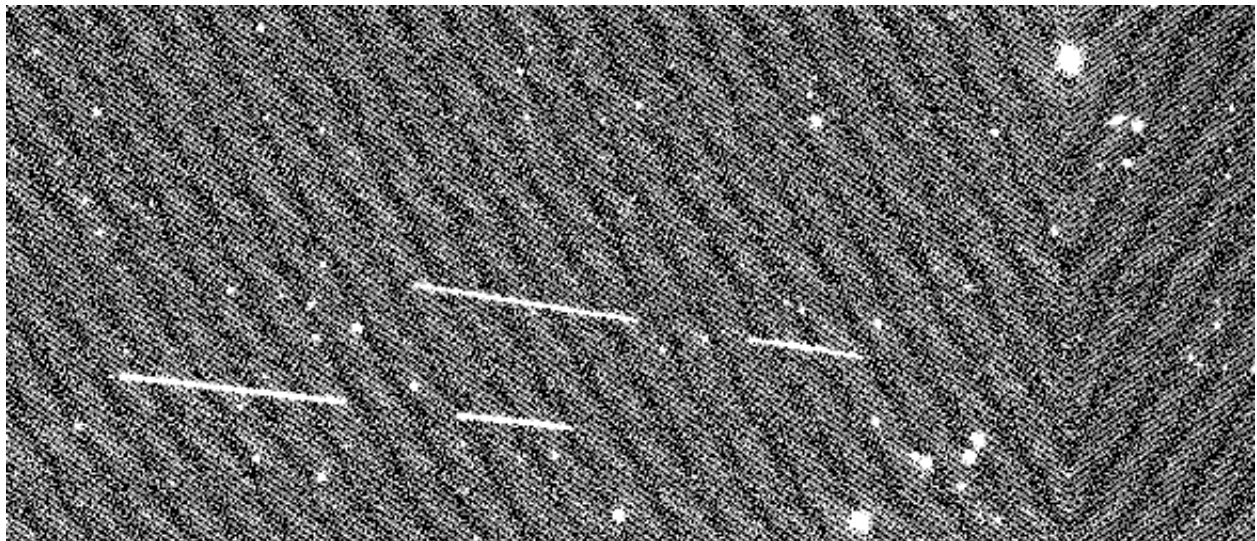


FIG. 11.—NEAT image of artificial satellites. Gaps appear in the streaks when shutter was held closed.

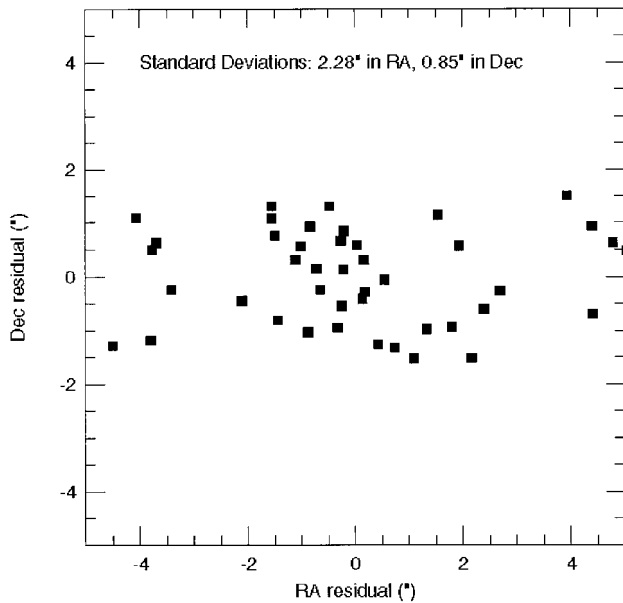


FIG. 12.—Observed minus predicted positions for artificial satellites observed with the NEAT system.

satellite orbits were known, these residuals show the measurement precision (both in position and time). It is apparent the measurement precision is  $\sim 1''$  in declination, and  $\sim 2''$  in right ascension. These tests also demonstrated the throughput of the NEAT observing program. With one satellite per image, a satellite position could be measured 40 times per hour, 2–3 times faster than the current GEODSS system.

## 5. DISCUSSION

### 5.1. Relative Limiting Magnitudes

The magnitude limit,  $V_l = 19.1 \pm 0.1$ , derived in § 4.2 is a reasonable result given the limit,  $V_l = 20.6 \pm 0.2$ , achieved by Spacewatch with their 0.9 Newtonian prior to 1992 September (Rabinowitz 1994). The Spacewatch limit has since been improved with the use of a more sensitive CCD and corrective optics. However, we restrict our comparison to the older system because it serves a good standard, and because Rabinowitz (1991) presents an analysis of the factors determining that limit. If two detector systems, 1 and 2, have CCDs with the same quantum efficiency and spectral response, use telescopes of the same aperture and reflectivity, observe through skies of the same brightness, and if dark current and read noise are negligible for both systems, then the difference in their limiting magnitudes,  $\Delta V$ , is given by

$$\Delta V = 1.25 \log [(t_1 p_2)/(t_2 p_1)], \quad (1)$$

where  $t_1$  and  $t_2$  are the exposure times, and  $p_1$  and  $p_2$  are the areas of sky covered by the CCD image of a typical star (including the full area of pixels only partially covered) for the respective systems. From Rabinowitz (1991), we have  $t_1 = 165$  s and  $p_1 = 13.14$  arcsec<sup>2</sup> ( $3 \times 3$  pixels) for Spacewatch, and for NEAT we have  $t_2 = 20$  s and  $p_2 = 8.12$  arcsec<sup>2</sup> ( $2 \times 2$  pixels). Hence, if the assumptions going into equation (1) were valid, NEAT would achieve a magnitude limit 0.88 brighter than Spacewatch, or  $V_l = 19.7 \pm 0.2$ . However, the NEAT limit is brighter than this initial esti-

mate because the dark current for NEAT camera is significant, whereas it is negligible for liquid-nitrogen cooled Spacewatch camera. At the nominal operating temperature near  $-3^\circ\text{C}$ , the measured dark current is  $\sim 90\text{ e}^- \text{ s}^{-1} \text{ pixel}^{-1}$  for NEAT, a factor of 1.3 higher than the measured sky background ( $69\text{ e}^- \text{ s}^{-1} \text{ pixel}^{-1}$ ). Furthermore, the dark current varies from pixel to pixel by an amount that is much larger than its own Poisson variation (square root of the integrated count per pixel). Our analysis software removes this nonuniformity from each search field by subtracting dark images of equivalent exposure time. Hence, the contribution of image noise to NEAT's magnitude limit is larger by a factor of  $(2 \times 1.3 + 1) = 3.6$  than the contribution of image noise to the Spacewatch limit, for which the sky noise is the only contributor. Incrementing our estimate of  $\Delta V$  by  $1.25 \times \log(3.6)$  yields the estimate  $V_l = 19.0 \pm 0.2$  for NEAT, consistent with our measured value.

### 5.2. Relative Detection Rates

Equation (1), above, also helps to explain NEAT's advantage with respect to Spacewatch for detecting NEAs larger than  $\sim 1$  km. As  $t$  is shortened, the sky area,  $S$ , that can be searched in a given time interval increases proportionately. Even though  $V_l$  decreases, thereby decreasing the apparent sky density,  $D$ , of NEAs, the product  $S \times D$  increases, thereby increasing the detection rate of NEAs. This is confirmed by the results of the Spacewatch and NEAT searches, which determine  $D$  as a function of  $V$ . As described in Rabinowitz (1994), Spacewatch observed  $1.8 \pm 0.6$  large NEAs ( $H < 18$ ) per 1000 deg<sup>2</sup> in a search to limit  $V_l = 20.6 \pm 0.2$  prior to 1992 September (a total of nine were detected in 4843 deg<sup>2</sup>). Given the value  $D = 0.78$  per 1000 deg<sup>2</sup> observed by NEAT at  $V_l = 19.1$ , and assuming  $D$  is proportional to  $b^V$ , then  $b = 1.8 \pm 0.2$ . Hence, for NEAs larger than  $\sim 1$  km, the total detection rate for a given system goes as  $[1.8^{1.25 \log(t)}]/t$  or  $(1/t)^{0.7}$ . Taking into account the respective field sizes (2.6 and 0.34 deg<sup>2</sup>), exposure cycle times (45 and 140 s), nights per run (6 and 18), and the limiting magnitudes (19.1 and 21.5) for NEAT and the current Spacewatch system (J. V. Scotti 1998, private communication), the relative detection rate of large NEAs should be  $(6/18) \times (2.6/0.34) \times (140/45) \times 1.8^{19.1-21.5} = 1.9$ . This is consistent with the detection ratio  $7/4 = 1.8$  for large NEAs given by Table 4, given the sampling error (60%).

### 5.3. Satellite Tracking Potential

The results of the satellite observations discussed in § 4.8 show that the NEAT system has a satellite tracking performance that exceeds the dynamic range, precision, and throughput of the current USAF operational system, a high-voltage video-tube-based instrument. The limiting magnitude for the operational instrument is about  $V = 15$ , while NEAT is able to detect satellites at least 3 mag fainter. With one satellite per image, the throughput of NEAT is 2–3 times faster than the current GEODSS system. Another advantage of the NEAT system is the capability of observing several satellites per exposure. Typical GEODSS procedures generate track data on only one satellite in the field of view at any one time, regardless of how many satellites are visible in the image. Processing of NEAT data, however, allows multiple tracks to be obtained per image. This is similar to asteroid observations, which can be processed to obtain track data on multiple asteroids per image. With an

algorithm that schedules satellite observations so that multiple satellites appear in the field of view, the throughput of such a system can be increased several fold. Furthermore, the test observation described in § 4.8 were made prior to improvements in the control program allowing telescope repositioning during image readout and allowing off-line descrambling. Combining these latest improvements with careful scheduling, the NEAT system offers a dramatic increase in throughput relative to current GEODSS procedures.

#### 5.4. The NEAT Network

NEAT is a prototype for an expanded network of similar systems, capable of fulfilling NASA's goal to detect and catalog at least 90% of the 1 km and larger NEAs by 2010 (Spaceguard Survey Report 1992; NEO Survey Workgroup Report 1995). Here, we estimate the capabilities of a network of three NEAT cameras, each operating on a different 1.0 m GEODSS telescope, and each allowed 18 nights per run to conduct the search. Such a system would displace the video-based cameras currently used at these telescopes to track artificial satellites. However, given the success of the satellite observations described in § 4.8, this system would be capable of both tasks.

The goal to find 90% of the large NEAs in 10 years can be restated as a target detection rate,  $R$ , of both new NEAs and incidental detections. Assuming a constant and random detection probability,  $r$ , per unit time,  $t$ , for each NEA, then the number of undiscovered NEAs will decrease with time as  $N_0 e^{-rt}$ , where  $N_0$  is the number that are undiscovered at  $t = 0$ . Already 227 NEAs larger than 1 km are known, and the estimated total population is  $N = 1000\text{--}4000$  (Shoemaker et al. 1979; Rabinowitz et al. 1994), so  $N_0 = N - 227 = 773\text{--}3773$ . Then to have 10% of the total population (100–400 objects) remaining undiscovered after 10 years requires  $r = \ln(N_0/0.1N)/10 = 0.205\text{--}0.224 \text{ yr}^{-1}$ . Hence,  $R = Nr = 200\text{--}900$  NEAs per year. At the current discovery rate of 36 large NEAs per year, it will take 60–250 yr to accomplish this goal. Preliminary results of Rabinowitz et al. (1998) from recent NEAT and other data indicate a flattening of the  $N$  versus  $H$  curve for these objects and point toward the lower number bound and thus shorter timescale for discovery.

With a network of three NEAT systems operating, and without any improvements to the camera and telescope systems, the situation improves but the detection rate still falls short of that required. Assuming 60% clear weather per telescope site (Maui is about 65% but other sites may be less), and assuming a practical limiting area of  $16,000 \text{ deg}^2$  per month, each telescope would be required to search an average of  $494 \text{ deg}^2$  per night or  $49.4 \text{ deg}^2 \text{ hr}^{-1}$ . With a field size of  $2.6 \text{ deg}^2$ , this translates to 19 triplets per hour, or 63 s per image. The overhead per image with the current NEAT system is 25 s, so this cycle time would allow exposure times of 38 s. The limiting magnitude would therefore increase by  $1.25 \log(38/20) = 0.3 \text{ mag}$  to  $V_i = 19.4$ . Our detection rate near the ecliptic of NEAs of more than 1 km would increase from the current value by the factor  $1.8^{0.3}$  to 0.93 per 1000  $\text{deg}^2$  (see § 5.2). Far from the ecliptic, however, we can expect a lower detection rate, as illustrated by our results presented in § 4.6. Whereas we detect NEOs at an approximately constant detection rate for  $\sin(\text{lat}) = -0.3$  to  $0.3$ , at higher latitudes our detection rate for NEAs larger than 1 km drops by a factor of  $\sim 3$  to  $0.3 \pm 0.2$  per 1000  $\text{deg}^2$  (we

detected two in a search of  $7200 \text{ deg}^2$  with  $\sin(\text{lat}) > 0.3$ ) Averaged over all sky area in the searchable range  $\sin(\text{lat}) = -0.3\text{--}1.0$ , our detection rate of these large NEAs is about  $60\% \pm 10\%$  of the rate near the ecliptic. This is consistent with the predictions of Bowell & Muinonen (1994), who show that the apparent sky-plane density of NEOs at  $\text{lat} = 30^\circ$  and  $60^\circ$  should be 60% and 40%, respectively, of the apparent density on the ecliptic for  $V_i = 18$  and 20. Hence, the yearly detection rate of NEAs larger than 1 km for a nearly full-sky search of  $16,000 \text{ deg}^2$  per month would be about  $0.6 \times 0.93$  NEAs per  $1000 \times 16,000 \text{ deg}^2 \times 12$  months per year = 110. At this rate, the time to 90% detection of the large NEAs would be 20–80 yr.

With some simple improvements to the camera and telescope system, the goal of a 10 yr program can be met, at least at the lower bound of the NEA number range. By cooling the NEAT cameras to  $-30^\circ \text{C}$ , the dark current would become negligible compared to the sky noise. This would increase  $V_i$  by 0.7 mag (see § 5.1). By reducing the overhead in the exposure cycle by 5 s, this would allow an additional 5 s per exposure, thus increasing  $V_i$  by 0.07 mag. Finally, by reducing the tracking error of the GEODSS telescopes, which currently causes images to trail in R.A. by 2 or more pixels, the spot size of image would be reduced by at least a factor of 2. This would increase  $V_i$  by 0.37 mag. Together, all these improvement increase the NEAT sensitivity by 1.1 mag to  $V_i = 20.5$ . The sky density of NEAs larger than 1 km then increases by  $1.8^{1.1} = 2.0$ , and the total detection rate increases to  $200 \text{ yr}^{-1}$ . At this rate, 90% of the 1000–4000 NEAs of more than 1 km would be discovered in 10–40 yr.

## 6. CONCLUSIONS

In the foregoing discussion, we have described the construction and operation of the NEAT system and documented the performance in terms of limiting magnitude, detection efficiency, rate of sky coverage, and detection rate. We have also discussed the capabilities of the system for satellite tracking. Compared to all other search programs, NEAT is the best for detecting the largest and most hazardous NEAs. Given only six nights per observing run, it is remarkable how well this system has competed with other systems with unlimited telescope access. Based on an analysis of the factors limiting the sensitivity of the current system, and of the factors affecting NEA discovery rates, we have predicted the performance of a NEAT network consisting of the existing system operating on a total of three GEODSS telescopes. With small improvements to lower the sensor temperature marginally, to reduce the exposure cycle time and to reduce the tracking error of the telescope, such a system would meet the challenge of detecting within the next decade most of the NEAs posing a long-term threat to civilization.

The NEAT team thanks B. Marsden and G. Williams of the Minor Planet Center for their invaluable help in identifying and categorizing asteroid and comet discoveries. We also thank D. Yeomans and M. Keesey for assistance in orbital determinations. NEAT would not be possible without the partnership of the USAF and the cooperation of their contractor PRC, Inc. In particular, we acknowledge Lt. Col. C. Bennet (Ret.), Lt. Col. L. Johnson, M. Endres, and A. Esquivel.

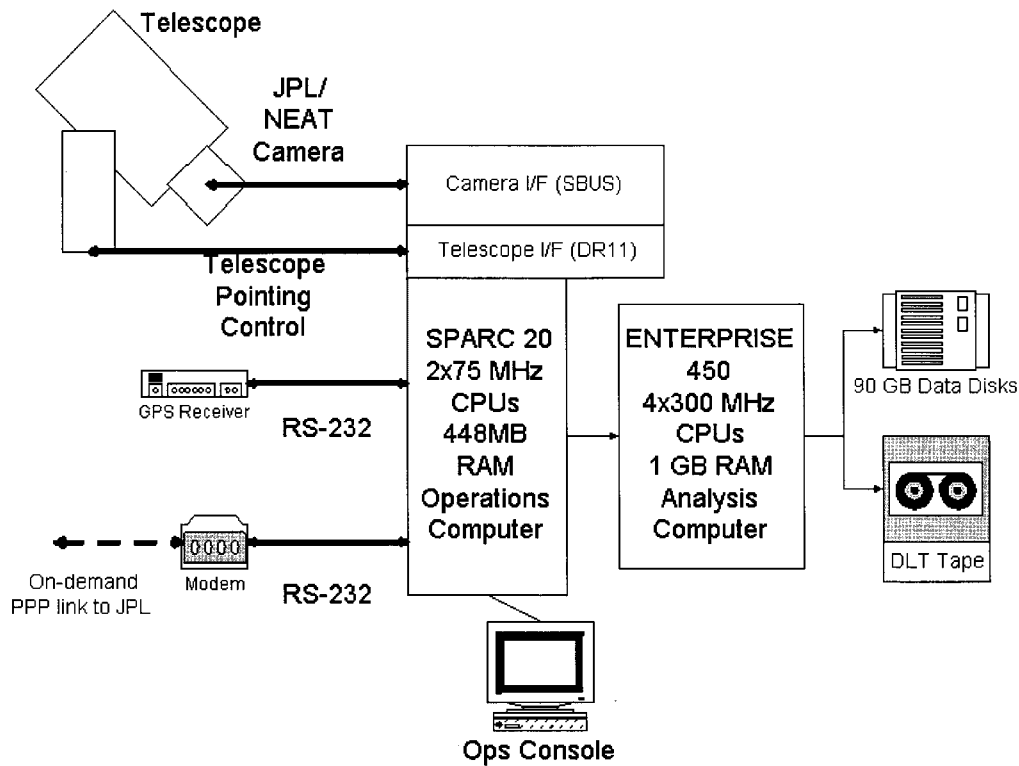


FIG. 13.—Hardware configuration

## APPENDIX A

### OPERATIONS SYSTEM

NEAT is an autonomous system. This enhances its efficiency and dramatically reduces personnel and travel costs since there are no on-site observers. Figure 13 shows the hardware associated with the observing functions (see text). All input and output data are transferred via modem using a commercial (800) number. The set of tasks comprising one night of observations is described in the following.

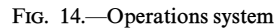
#### A1. OBSERVING SCRIPT AND NEAR-REAL-TIME OBSERVATIONS

The observing script is uploaded daily via the modem connection between the NEAT operations computer and JPL. Each line consists of an R.A. and decl. position, a character indicating whether or not to open the shutter, the exposure time, the interval between exposures, the number of exposures, an optional time to perform the observation, and a comment. The first line is the request for dark observations. For these the pointing position is irrelevant (set to 0.,0.) and the shutter does not open. The exposure time is set to 20 s, the same as that for the later celestial observations. Darks are taken in 1 hr intervals. The next set of requested observations are survey observations. They cover a grid in the sky starting at and extending from the ecliptic plane and in increasing R.A. order. Follow-up observations have comments in the last column indicating the target and its properties. The observing script can be updated in real-time using the SUBMIT command. This allows the user to input an observation in the same format it would appear in the observing script. This new observation is then incorporated into the existing script by the SUBMIT process.

#### A2. OBSERVING SCENARIO

Late in the day before NEAT observations are scheduled to begin, the program GETSEQUENCE is run on the operations computer to telemeter the nights observing script from JPL to Maui. Next the program PRERUN is executed to prepare the hard disks for new observations and data. These tasks take about 5 minutes. At astronomical twilight on-site personnel remove the telescope cover (the only task that can not be performed remotely) and begin the observing program. Barring interruptions from weather or equipment problems, on-site personnel are not further tasked until astronomical dawn.

A number of real-time software "managers" run during operations to control the hardware and data flow. Figure 14 shows the software design by real-time element. The real time programs are written and compiled in C, while the analysis programs are FORTRAN and C. NEATCTL is the top-level program. Under it is the schedule manager (SCHEDMGR) that organizes the observing script, keeps track of the observations completed and to be done, and creates the queue for analysis. SCHEDMGR tells the observations manager (OBSMGR) the next observation to perform. OBSMGR passes on the observing request to the telescope manager (TELEMGR). TELEMGR points the telescope, moves the dome, and sidereally tracks at the positions provided by OBSMGR. After TELEMGR moves the telescope to the requested position, it informs OBSMGR of that fact. OBSMGR then commands the camera to open shutter, take an exposure, close shutter, and download imaging data to hard disk. It then informs SCHEDMGR that the observation is completed. SCHEDMGR updates its checkpoint file of completed



### A3. TIMEKEEPING

#### A4. OPERATIONS STOP, DATA TRANSMISSION, AND ARCHIVING

The extra time afforded because of efficient data analysis has also allowed improvement in the data archiving. There is now time to compress the raw image data by a factor of 2 using a fast algorithm developed for NEAT by M. Klimesh of JPL. This algorithm losslessly compresses a 33 MB image file in less than 10 s on the Enterprise 450. The DLT archive rate of about 5 MB s<sup>-1</sup> then allows a timely backup of the data. Two to three nights of data fit onto one DLT tape, which has a capacity of 35 GB.

# ASTEROID DETECTION SOFTWARE

NEAT's goal is discovering new NEOs. Data from the detections each night must be analyzed *and disseminated* for follow-up observations the next night with NEAT or by other observers. Analysis thus occurs in real time or near-real time



depending upon the backlog of analysis units. An analysis unit consists of three sky images with almost the same center and orientation taken 10 minutes or longer apart. Since each image consists of about  $1.6 \times 10^7$  pixels, each 2 bytes, an analysis unit is  $\sim 100$  MB of data. The following subroutines execute:

1. REMDARK subtracts the nearest dark (exposure with the shutter closed) in time from each of the images. Bad pixels—about 0.25% of the total—are also removed.

2. ORDSTAT computes statistics from the dark-subtracted images such as the average count rate and the count rate moments. Since each quadrant of the CCD has its own output amplifier (see text), statistics for each are calculated separately. A local background is computed in each few hundred pixel area and subtracted to flat-field the image (see § 2.3).

3. STARCAT finds the objects in the three images. Objects have count rates that are larger than  $N_1$  sigma over local median, and consist of  $N_2 \times N_3$  contiguous pixels, where the  $N_i$ -values are selectable. Current values of  $N_i = 3, 2, 1$  strike a balance detecting enough real objects just above the background and not too many false objects. For each object STARCAT records its catalog entry number, sum of data numbers minus background (=intensity), number of pixels, starting X-value, starting Y-value, X length, Y length, X center, Y center, major axis length, minor axis length, ratio of minor to major axis, and rotation angle of ellipse. The number of objects found in each field range from 3000 to more than 10,000 as the Galactic latitudes decrease. For latitudes less than about  $10^\circ$ , the number of stars in the Galactic plane gets so large that the analysis takes longer with less chance of success because of source confusion. These latitudes are avoided in the search program. For the middle image STARCAT repeats the object finding at a lower threshold,  $N_1 = 2.5$ . This list of objects is used as a fiducial. At this point, the analysis is finished with the image data until the final step. All further analysis is performed on the tables of output data that consist of the lists of objects, their pixels positions, their shapes (length and width), and their intensities.

4. RMSCHK looks at the root mean square (rms) of the objects numbers found in the three images. If this number is larger than a threshold of several thousand, then the analysis is aborted. This can happen if the weather is variable and the scene becomes very cloudy in one of the images, or if there is some camera failure, e.g., the shutter did not open. On a clear night, rms will range from less than one hundred to several hundred.

5. TABREG registers the first and third images to the second image by cross-correlating the detected objects. Although the pointing position and orientation are closely reproduced, small offsets of order arcminutes of translation are introduced by the telescope and pointing system. For completeness TABREG solves for the six coefficients of a general transformation that best overlays the images. The only significant coefficients, however, are the X and Y translations. Their starting values are estimated accurately as the maxima X- and Y-values of the histogram of offsets between all the objects in the two tables. The other four parameters account for scale changes (perhaps due to focus drift) and rotations. These are insignificant (amounting to contributions smaller than 1 pixel) even on the edges of the field where their effects are maximal. A least squares fit using the 100 brightest objects in each table solves for the final values.

6. TABMATCH compares the image tables to eliminate stationary objects—stars and galaxies. It creates three final output tables corresponding to the objects in image 1 only, image 2 only, and image 3 only. TABMATCH operates on two input tables at a time. It first geometrically registers the inputs tables to each other by using the coefficients derived in TABREG. The output table consists of all objects that are found in the second input table AND not in the first input table. Objects in the two input tables are considered the same and thus eliminated from the output table using one of two criteria: their centroids are within  $N_4$  pixels of each other, or their areal locations overlap. In practice it was found that the second option eliminated bright, slow moving asteroids and comets, so the first option is used with  $N_4 = 3$ . After six applications of TABMATCH the three final output tables are produced.

7. TABEDIT edits the output tables of TABMATCH to eliminate “clusters” of objects. Clusters are defined herein as more than one object in a 20 pixel radius. These were found to be almost exclusively due to the diffraction spikes around bright stars and their elimination resulted in considerably less candidate objects.

8. NEOFIND uses as inputs the three output tables of TABMATCH and TABEDIT. For each pair of objects, the first from output table 1 and the second from output table 3, NEOFIND searches output table 2 for an object that is within  $1''/8$  of their interpolated linear motion. If an object is found in table 2, then the three objects are output as a candidate asteroid or comet. NEOFIND limits the pairs of objects to within a 300 pixel search radius of each other, which at the typical NEAT reobservation interval corresponds to objects moving less than  $6^\circ \text{ day}^{-1}$ . Since the maximum velocity of any object detected with NEAT has been below this threshold, the time saved in limiting the search (which increases with the square of the search radius) has little consequence in objects not detected.

9. If no asteroid/comet candidates are found the processing stops. Otherwise TABMAP finds the fields from the Guide Star Catalog (1989) that overlap the image based upon the nominal pointing position. This nominal pointing position is accurate to  $\sim 0''.1$  or less, much smaller than the NEAT or guide star fields. TABMAP compiles a list of the guide stars and their positions from these fields.

10. STARREG finds the 1000 brightest stars from the table of the second image and correlates them with the guide stars to solve for a six-parameter (three in each dimension) transformation between pixel  $[X, Y]$  and  $[R.A., \text{decl.}]$ . The parameters account for translation, rotation, and scale changes and are fitted only after the effect of distortion is removed and the field is “linearized.” This is a multistep process because the GEODSS field has significant optical aberrations at the edges. The important aberration is distortion whose affect is to cause a cubic deviation from linearity with radius of object positions. While the magnitude of this term is well-measured, the phase depends upon the center of the field, which changes depending on slight differences in the mounting of the camera on the telescope (of order  $100 \mu\text{m}$ ). The aberration adds to the effects of the translation, rotation, and scale change, and all are required to fit the guide stars to the NEAT bright stars. The method used is to first correlate the brightest stars in the central 2000 pixels where the field is nearly linear. From this the center of the field is

calculated. This center is then used with the known magnitude of the distortion and, as a starting point, the six coefficients determined in this previous step to fit the stars in the central 3000 pixels. The fit is bootstrapped until the entire field is correlated with guide stars. The astrometric precision is of order 0".3.

11. ASTROM applies the coefficients calculated in STARREG to transform the  $[X, Y]$  positions of the moving object candidates into  $[R.A., decl.]$ .

12. NEOEDIT compares the three looks at each candidate moving object. If the variations in intensity, shape (ratio of minor-to-major axes), or orientation (rotation angle of ellipse) exceed their thresholds, the candidate is rejected. The severity of these thresholds were adjusted empirically so that real objects were not eliminated. In practice this editing rejects less than 50% of the candidates.

13. Finally, PATCHES goes back to the original images and extracts a small square area around each candidate (typically 18 or 25 pixels on a side) at each of the three  $[X, Y]$  positions and from each of the three images. These subimages are reduced to 8 bits per pixel. Every candidate object is thus represented by nine subimages. These are arranged for postanalysis as shown in Figures 3 and 4. These "patches" are a most important part of the postanalysis providing a sanity check for the reality of objects and a means of detecting comets. The number of false positives revealed by PATCHES is entirely dependent on processing parameters chosen in the steps listed above. We are able to tune the percentage of false positives to between 20%, which is too restrictive, and 95%, which is too inclusive. The parameters we decide upon finally are those for which the number of false positives does not overwhelm our data screeners, also a function of the total data throughput. A typical percentage is 80%.

14. An analysis unit takes anywhere from 2 to 10 minutes to run on a dedicated CPU, depending upon the CPU speed and the I/O environment. For the current real-time analysis computer with 300 MHz processors, the time is near the lower end of this range. Approximate percentages of time spent in each of the steps listed above are REMDARK, 14%; ORDSTAT/STARCAT, 47%; TABREG/TABMATCH/TABEDIT, 20%; NEOFIND, 4%; STARREG, 4%; ASTROM, 3%; and PATCHES, 4% (with another 4% spent cleaning up files).

#### REFERENCES

- Bowell, E., & Muinonen, K. 1994, in *Hazards Due to Comets and Asteroids*, ed. T. Gehrels (Tucson: Univ. Arizona Press), 149
- Davies, J. K., McBride, N., Green, S. F., Mottola, S., Carsenty, U., Basran, D., Hudson, K. A., & Foster, M. J. 1998, *Icarus*, 132, 418
- Drummond, J., & Rabinowitz, D. 1993, in *Resources of near-Earth space*, ed. M. S. Matthews & M. L. Guerrieri (Tucson: Univ. Arizona Press), 449
- Gehrels, T. 1994, in *Hazards Due to Comets and Asteroids*, ed. T. Gehrels (Tucson: Univ. Arizona Press), 1
- Guide Star Catalog. 1989 (Baltimore: SSTScl)
- Helin, E. F., Pravdo, S. H., Rabinowitz, D. L., & Lawrence, K. J. 1997, *Ann. NY Acad. Sci.*, 822, 6
- Hicks, M. J., Buratti, B. J., Newburn, R., & Rabinowitz, D. 1998, *Icarus*, submitted
- Jedicke, R., & Herron, J. D. 1997, *Icarus*, 127, 494
- Leach, R. W. 1996, *Proc. SPIE*, 2654, 218
- McFadden, L., Tholen, D. J., & Veeder, G. J. 1989, in *Asteroids 2*, ed. R. P. Binzel, T. Gehrels, & M. S. Matthew (Tucson: Univ. Arizona Press), 442
- Minor Planet Center. 1999, <http://cfa-www.harvard.edu/iau/NEO/TheNEOPage.html>
- NEO Survey Workgroup Report. 1995, ed. E. Shoemaker (Washington: GPO)
- Pravdo, S. H., Helin, E. F., Rabinowitz, D. L., Lawrence, K. J., & McGlynn, T. A. 1998, *BAAS*, 192, 900
- Rabinowitz, D. L. 1991, *AJ*, 101, 1518
- . 1993, *ApJ*, 407, 412
- . 1994, *Icarus*, 111, 364
- . 1997a, *Icarus*, 127, 33
- . 1997b, *Icarus*, 130, 287
- Rabinowitz, D. L., Bowell, E., Shoemaker, E. M., & Muinonen, K. 1994, in *Hazards due to Comets and Asteroids*, ed. T. Gehrels (Tucson: Univ. Arizona Press), 285
- Rabinowitz, D. L., et al. 1998, in *Catastrophic Disruptions Workshop 5*, (Mt. Hood)
- Rabinowitz, D., Helin, H., Pravdo, S., & Lawrence, K. 1996, *BAAS*, 28, 1096
- Scotti, J. V., Gehrels, T., & Rabinowitz, D. L. 1991, in *Asteroids, Comets, Meteors*, ed. A. Harris & E. Bowell (Houston: Lunar and Planetary Inst.), 541
- Shoemaker, E. M., Williams, J. G., Helin, E. F., & Wolfe, R. F. 1979, in *Asteroids*, ed. T. Gehrels (Tucson: Univ. Arizona Press), 253
- Spaceguard Survey Report. 1992, ed. D. Morrison (Washington: GPO)
- Weissman, P. R., & Levison, H. E. 1997, *ApJ*, 488, L133